P58

NASA
Technical
Paper
2888

April 1989

Evaluation of Cloud Detection Instruments and Performance of Laminar-Flow Leading-Edge Test Articles During NASA Leading-Edge Flight-Test Program

Richard E. Davis, Dal V. Maddalon,
Richard D. Wagner, David F. Fisher,
and Ronald Young

Date for general release   April 30, 1991

NASA

NASA
Technical
Paper
2888

1989

Evaluation of Cloud Detection Instruments and Performance of Laminar-Flow Leading-Edge Test Articles During NASA Leading-Edge Flight-Test Program

Richard E. Davis, Dal V. Maddalon, and Richard D. Wagner
Langley Research Center
Hampton, Virginia

David F. Fisher and Ronald Young
Ames Research Center
Dryden Flight Research Facility
Edwards, California

Contents

Nomenclature

A width of photodiode array in Knollenberg probe, 30 μm

ACEE   Aircraft Energy Efficiency Program (NASA)

ASA   actual sampling area of Knollenberg probe, mm^2 (see appendix C)

ATL   Aerodrome designator for Atlanta, Georgia

av   average

C_Z ambient particle concentration in probe size channel Z, m^{-3} (see appendix C)

CA   clear air

$\overline{CA}$ unclear air

CLE   Aerodrome designator for Cleveland, Ohio

C0   percentage of time on flight having zero particle concentration

c.patch   charging patch

c total wing chord, ft (see appendix A)

D depth of field for Knollenberg probe, mm (see appendix C)

DFRF   Ames Research Center, Dryden Flight Research Facility

DOC   Direct Operating Cost

EMD   equivalent melted diameter (of ice particle), μm

F_Z sampling effectiveness factor in size channel Z of Knollenberg probe, knot-sec-m^{-3} (see appendix C)

f focal length

H effective width of Knollenberg probe sampling array, mm (see appendix C)

h_p pressure altitude, ft

K.probe   Knollenberg probe

L arbitrary specified value of LF in testing of particle detectors as LF-diagnostic devices

LEFT   Leading-Edge Flight-Test Program (NASA)

LETA   Leading-Edge Test Article

LF   laminar flow; also used as variable denoting areal percentage of laminar flow over a leading-edge suction test article

LFC   laminar-flow control

M_∞ free-stream Mach number

max   maximum

min   minimum

N total number of photodiodes in Knollenberg probe, 32 (see appendix C)

OAP   Optical Array Probe (PMS, Inc.)

obs   observations

$P(\ )$ probability of occurrence of event ( )

$P(a|b)$ conditional probability that event a will occur given that event b has occurred

$P_{Z,T}$ number of particles sampled in a given time interval T in channel Z by the Knollenberg probe (see appendix C)

PIT   Aerodrome designator for Pittsburgh, Pennsylvania

PMS   Particle Measuring Systems, Inc.

$p_{t,probe}$ total pressure, measured at near-surface pitot probe, lb/ft^2

$p_{t,\infty}$ free-stream total pressure, lb/ft^2

q dynamic pressure, lb/ft^2 (see appendix A)

R statistical correlation coefficient, $-1 \leq R \leq +1$

r radius of particle, μm (see appendix C)

SAS   Simulated Airline Service

SPSS   Statistical Package for the Social Sciences

SRI   Stanford Research Institute

T elapsed time between measurements, sec (see appendix C)

TAS	true airspeed, knots	Z	designator of size channel for Knollenberg probe, $Z = 1, 2, \ldots, 30$ (see appendix C)
USAF	<u>U</u>nited <u>S</u>tates <u>A</u>ir <u>F</u>orce		
V_∞	free-stream velocity, knots	Z0	percentage of time in zero-range conditions
x	distance from wing leading edge to point on chord, $x \leq c$, ft (see appendix A)	Δp	measured pressure differential, $p_{t,\infty} - p_{t,\text{probe}}$, lb/ft^2 (see appendix A)
x/c	fraction of chord, dimensionless (see appendix A)	Subscripts:	
		L	level of laminar flow
Y	number of photodiodes occulted by particle (see appendix C)	tr	flow transition

Summary

The degradation of laminar flow over aircraft surfaces within clouds and haze is a subject of concern in assessing the viability of laminar-flow-control aircraft concepts. Therefore, statistics summarizing the performance of prototype leading-edge laminar-flow-control devices on the NASA JetStar aircraft during 19 flights in the Leading-Edge Flight-Test (LEFT) Program are presented. The results, differentiated into clear air, haze, and cloud conditions, show that there was significant loss of laminar flow while the aircraft was within cloud or haze conditions and that the loss of laminar flow is correlated with an increase of particle size and/or particle concentration. Two instruments—a laser particle spectrometer (Knollenberg probe) and a charging patch, which infers the presence of cloud particles through their triboelectric effect—were used to monitor the ambient haze-cloud particle environment. The suitability of each of these instruments as a diagnostic aid for avoiding particle concentrations detrimental to laminar flow is evaluated; it is concluded that, while both instruments are suitable in this application, the charging patch is particularly suitable due to its ruggedness and simplicity.

Introduction

Fuel cost is a major factor in airline direct operating cost (DOC), and variability of fuel cost has also been a problem for airline economic planning. Fuel costs were at only 35 percent of DOC at the start of the 1973 oil embargo, rose to near 60 percent in the early 1980's (ref. 1), and were reported to be near the 55-percent level in 1984 (ref. 2). Although the present numbers are likely to be less than this, future values remain uncertain, and methods for reducing fuel consumption are therefore of great importance in airline operations. Future advanced transports will incorporate advanced technologies which can reduce drag and weight and lower fuel consumption (ref. 3). One promising technology for drag reduction and fuel saving is laminar-flow control (LFC). Research into the concept of laminar boundary-layer control can be traced back to the 1930's and 1940's, when both theoretical analysis and experiments were carried out (ref. 3). The concept of suction-stabilized laminar-flow control is shown in figure 1. In figure 1(a), the airflow around a current standard (i.e., turbulent) wing is shown. The flow is laminar over a very limited extent of the chord; then transition to turbulent flow takes place. In figure 1(b), suction (through slots or perforations in the surface) is employed in a carefully tailored fashion such that the boundary layer remains stable and laminar over a larger ex-

tent of the chord before becoming turbulent. International research in laminar flow continued into the 1960's, culminating in the United States with the USAF-sponsored X-21 program (refs. 4 and 5). The X-21 flight tests confirmed that extensive laminar flow could indeed be achieved at subsonic transport cruise conditions but also showed that there still remained unresolved concerns, both on manufacturing and on environmental levels, as to the viability of the LFC concept in operational service. On the manufacturing side, there was concern regarding the practicality of constructing wing surfaces (with the technology then available) which would meet the stringent smoothness and waviness criteria and which would maintain this surface quality in operational service. On the environmental level, there was the concern that insect impingement and other surface contamination on the wing surface could reduce LFC efficiency and also the observation, in X-21 operations, that encounters with clouds—even tenuous ones— adversely affect the maintenance of laminar flow. It is the latter concern—cloud effects on LFC which motivated the research reported here.

In response to the fuel crisis, NASA initiated efforts in 1976 in laminar boundary-layer control for drag reduction as part of the Aircraft Energy Efficiency (ACEE) Program to develop new technology for fuel efficient commercial transports (ref. 6). This initiative used as a springboard the significant progress in structural materials, fabrication techniques, analysis methods, and design concepts that had occurred since the 1960's to develop improved LFC technology and provide evidence that practical, reliable, and maintainable systems were now within the state of the art. The most difficult problems in achieving laminar flow (LF) on commercial transports appear to be associated with the wing leading-edge region, which is the portion of the wing most subject to foreign object damage, insect impingement, rain erosion, icing, and other contaminants. Therefore, NASA conceived the Leading-Edge Flight-Test (LEFT) Program (refs. 3 and 7), a flight program to test the effectiveness of LFC systems developed with modern technology and to evaluate their reliability and maintainability.

Even with the hoped-for resolution of the concerns on the manufacturing-reliability-maintainability level, concerns on the effects of cloud particles on LFC remained. Therefore, it was necessary to evaluate the effects of clouds and haze on LFC systems during the LEFT Program. This evaluation proceeded in two stages. First, studies were performed to assess the a priori probability of cloud encounter at typical transport altitudes. The results of these empirical studies (refs. 8 and 9) basically

showed that cloud encounters would be expected only about 6 percent of the time at typical airline cruise altitudes and that it is therefore practical to consider LFC for future transports. Second, it was decided to fly cloud-detecting instruments aboard the LEFT research aircraft, to evaluate directly the effects of the dynamic behavior of the ambient cloud-particle concentrations on the concurrent extent of laminar flow on the aircraft. Therefore, two cloud-particle detecting instruments were flown aboard the JetStar aircraft. One of these is a commercially available laser particle spectrometer and the other is a charging-patch device. These are described in detail in this report.

The LEFT program began in 1983 and was completed during 1987. The results (refs. 10, 11, and 12) show that the program was a success on the operational level; that is, LFC is indeed a viable concept for transport application. The cloud-particle instrumentation also performed successfully. Preliminary results were presented in reference 13. The major goals in the present paper are to extend the results of reference 13 to cover the entire simulated airline service portion of the LEFT Program, document thoroughly the effects of clouds on the level of laminar flow obtained, and evaluate rigorously the performance of the cloud-particle instrumentation. This paper provides an archival document on the instrumentation and analysis procedures used to study the cloud problem; this document may serve as a useful reference in subsequent laminar-flow investigations.

Glenn R. Bittner and Richard S. Thompson of the Unisys Corporation, Hampton, Virginia, assisted in processing the data tapes sent to Langley from Ames-Dryden and in performing the statistical analyses needed for this paper.

Aircraft and LFC Test Articles

The LEFT aircraft is a modified Lockheed Jet-Star aircraft (NASA aircraft 814), from which the standard mid-wing slipper fuel tanks (i.e., flush with wing, not pylon mounted) have been removed and replaced by laminar-flow gloves, as shown in figure 2. Each glove consists of a fully functional leading-edge test article (LETA) and a fairing; each LETA includes a laminar-flow boundary-layer suction system, a cleaning/contamination prevention system, and an anti-icing system. Each LETA extends along about 6 ft of span and extends back to about 13 percent chord, and each glove is faired into the rear spar at about 60 percent chord (upper surface).

The two LETA's involve different concepts. The laminar-flow glove on the right wing incorporates a Douglas Aircraft Company laminar-flow concept

wherein the upper surface of the test article is perforated, with electron-beam-drilled holes of about 0.0025 in. diameter spaced about 0.035 in. apart. Boundary-layer suction on this test article is applied on the upper surface only, from just below the flow attachment line at the leading edge back to the upper front spar. Having suction on the upper surface only allows use of a Krueger flap (a type of leading-edge high-lift device), which also serves as an ice and insect protection shield. A spray nozzle is mounted on the underside of the Krueger flap to enhance insect and ice protection. Approximately 60 percent of the LETA surface is perforated; there are about 1 million holes in the test article. The Krueger flap, an integral part of the Douglas LFC concept, is used to lower the landing speed, but using such a flap removes the possibility of using LFC on the wing undersurface.

The left-wing glove incorporates a Lockheed Aircraft Corporation LFC concept which employs suction through very fine (0.004-in-wide) spanwise slots on both the upper and lower surfaces of the test article back to the front spar. There are 27 LFC slots, 6 of which in the attachment line region serve the dual purpose of dispersing a protective fluid film for insect protection and anti-icing.

Only a brief description of the LETA's has been given here; more details may be found in references 3, 7, and 13 through 18. Both LETA's have pressure-measurement instrumentation (surface pitot arrays, flush-mounted orifices, and hot-film sensors), arranged as shown in figure 3. The use of the pitot array sensors to derive LF measurements is described in appendix A. (Hot-film-sensor data were not used in this analysis.) The pitot measurements are used to derive an areal percentage of laminar flow on each LETA.

To avoid confusion, it should be stated that there are two LETA's, one slotted and one perforated, but in discussing the laminar-flow performance of the slotted LETA, separate results are given for the upper and lower surfaces. For the perforated LETA, which has only an upper surface, only one value is given. Thus, there are three values overall which describe the LF performance of the aircraft, at any point in time, in terms of areal percentage of laminar flow on each LETA surface. These are referred to in this report as the values for the slotted upper, slotted lower, and perforated surfaces. These values constitute the dependent variables for the later analysis, where cloud-particle concentration (or charging-patch current) constitute the independent variables.

Meteorological Effects on LFC

The concern about cloud-particle effects on laminar flow dates at least as far back as the early 1960's to the USAF/Northrop X-21 program (ref. 4). During flight testing at typical X-21 cruise conditions of $M_\infty = 0.75$ and $h_p = 40\,000$ ft, it was observed that laminar flow was totally lost whenever the aircraft penetrated cirrus clouds, with horizontal visibilities estimated to be about 5000 to 10 000 ft. Also, LFC performance was observed to be partially degraded or erratic when penetrating light cirrus "haze," even when the horizontal visibility was as much as 50 miles. Because both these effects were also expected to be present in the LEFT experiment, the decision was made to carry cloud instruments on the JetStar. At typical aircraft cruise altitudes, cirrus clouds and haze are composed mostly of ice crystals. These crystals have a detrimental effect on maintaining laminar flow, depending on their size and concentration (or flux, as perceived by the aircraft). To explain the erratic LFC performance in clouds and haze during the X-21 program, Hall (ref. 19) developed a theory (summarized here in appendix B) to predict the effects of ice-crystal encounter on the maintenance of laminar flow. Basically, Hall's theory postulates that ice particles entering the boundary layer shed turbulent vortices, which cause transition in the main flow, as shown in figure 4. The key factors which determine whether any given cloud encounter will cause total, partial, or negligible loss of LF are the cloud particles' size, concentration, and residence time in the boundary layer. Reference 15 notes that Pfenninger has suggested that wing sweep is also a key factor. This is because the spanwise flow on a swept wing may lead to greater particle wake velocity defects, which promote increased turbulence production, and also because the increased effective chord on a swept wing may result in higher particle residence times in the boundary layer. Also, compressibility effects encountered at high altitudes and high Mach numbers may cause some partial loss of laminar flow.

LEFT Particle Instrumentation

Need for Instrumentation

The need for instrumentation aboard an aircraft for discerning the presence of ambient particle concentrations is sometimes questioned, and therefore the utility of the two instruments discussed in this report for general LFC aircraft application may also not be apparent. This is because true (i.e., thick, opaque) clouds are obviously visible by an aircrew especially during daylight conditions. Haze, however, can be more difficult to detect, particularly when viewed in an azimuth opposite from the Sun direction. Also, it is frequently difficult to assess ambient cloud-haze conditions on dark nights. Therefore, it is believed that an instrument would be useful for detecting conditions that degrade LF but which are not obviously hazy to an aircrew. Having such instrumentation would enable the aircrew to determine that conditions are detrimental to maintaining maximum LF levels and to request altitude changes to restore maximum LF.

Figure 5 is an example of conditions in which haze, only barely apparent in a photograph, was degrading the level of LF on a JetStar mission in the LEFT Program (flight 1099). Both photographs in the figure were taken by the JetStar aircrew while looking out of the left side of the aircraft with the Sun behind the photographer; the left wing is apparent in each photograph. A haze condition, with its upper boundary approximately at the level of the tropopause, is apparent at about the elevation angle of the wingtip. The photograph in figure 5(a) was taken at 9:24:00 local time. Figure 5(b) is a photograph taken 9 minutes later at 9:33:00 local time. During the condition shown in part (a), the level of LF was 100 percent on the perforated article (less on the other article). In the condition in part (b), the level was 80 percent on the perforated article. However, the difference in haze conditions in the two photographs was not very apparent. This pair of photographs demonstrates that an instrument for detecting ambient particles would be useful to an aircrew.

The instrumentation for measuring the ambient atmospheric (cloud) particle environment during flights of the JetStar LFC aircraft consists of two instruments mounted on a pylon extending dorsally from the JetStar fuselage, as shown in figure 6. (This pylon was omitted from fig. 2 for clarity in showing the LETA's.) The two instruments are a well-proven cloud-particle spectrometer, commonly known as a Knollenberg probe, and a charging patch based on a triboelectric (frictional) charge-exchange principle. Both instruments measure the free-stream particle environment well away from any fuselage-induced concentration effects. These instruments are now described individually.

Cloud Particle Spectrometer (Knollenberg Probe)

A Particle Measuring Systems optical array cloud droplet spectrometer probe model OAP-230X, mounted atop the pylon in a cylinder (fig. 6), is used as a "truth" instrument to measure the spectra (number density vs. particle size) of cloud and other

particles encountered on the LEFT missions. Figure 7 shows the principle of operation (part (a)), a diagram of the probe optical system (part (b)), and a photograph of the probe in its housing (part (c)). Figure 7(a) is a snapshot view of a particle passing transversely through the laser beam with the free-stream velocity V_∞. While within the beam, the particle's cross section casts a shadow which is imaged on the elements in the photodiode array. From the number of elements shadowed at any instant, an estimate of the particle's transverse dimension is obtained. Several versions of the optical array probe (OAP) are available; the 230X version most nearly suited the requirement perceived for LEFT. The OAP-230X probe measures particles in 30 size bins between 20 and 600 μm effective size with a bin resolution of 20 μm. The instrument is designed to provide measurements in all 30 size channels at 100 m/sec (194 knots) free-stream velocity. However, because the JetStar flies at approximately 500 knots (258 m/sec), measurements in the first two size channels, 20–40 and 40–60 μm, are not obtained due to electronic response time considerations, but measurements of particles sized between 60 and 600 μm are obtained accurately. Appendix C provides additional detail on probe operation and derivation of particle concentration from the probe measurements. From Hall's theoretical analysis (ref. 19 and appendix B), particles larger than 33 μm should affect laminar flow at an altitude of 40 000 ft. (In ref. 19 it is also shown that particles larger than 18 μm should affect laminar flow at 25 000 ft.) Therefore, the probe will provide measurements of most, but not all, the particles that are predicted to affect LF; there appears no acceptable way around this dilemma because, although instruments exist for measuring particles smaller than 60 μm diameter, such instruments are based on a Mie-scattering-based interpretation of forward-scattered light data, which is valid only for spherical particles. When such forward-scattering probe instruments are used to measure ice particles, which commonly have a nonspherical form, the concentrations inferred may be in error by 1 to 2 orders of magnitude (ref. 20). For these reasons, the OAP-230X probe is used to give reliable measurements of particles of 60 μm EMD or larger; for the concentration of smaller sized particles, only a subjective extrapolation of the measured particle concentration curve is available. Aerodynamic considerations, based on references 21 and 22, suggest that the other instrument (charging patch) is affected by particles down to 20 μm in size. Thus, the readings of both instruments taken together can be used to infer the total particle environment. For example, on a few occasions during the JetStar flights,

readings were obtained from the charging patch when the Knollenberg probe showed that no particles were present in its effective range; this behavior indicates that the patch is indeed more sensitive to smaller particles than is the probe. In most cases, however, both patch and probe simultaneously indicated particles. The patch-reading-only cases are typical of very thin cirrus hazes with large horizontal visibility (several tens of miles), whereas the instances of simultaneous readings in both instruments are associated with visible clouds and haze. Spectrometers such as the OAP-230X probe used here have been successfully used by several researchers in airborne cloud research, most extensively in the USAF Cirrus Particle Distribution Study (e.g., refs. 23 and 24). Therefore, reliable results and straightforward data interpretation were anticipated and were, in fact, achieved. Additional detail on the theory of operation of spectrometer probes may be found in reference 25.

The probe weighs 45 lb and requires 60 W of 115-V, 400-Hz power for its operation and 70 W of 28-V dc power for its deicing system.

Data System

The output of the Knollenberg probe is fed to an onboard data system. An accumulating memory is provided so that the number of particles encountered in each size channel during a specified time interval is recorded, along with various other system outputs such as time code, on magnetic tape. For comparison to the charging-patch measurement, the difference in the accumulating count is calculated at 1-sec intervals.

An example of a particle count obtained during a typical visible cirrus cloud penetration is given as figure 8(a). The ordinate gives the 1-sec particle count and the double abscissa gives the channel and particle diameter in μm. The figure shows that particles were counted in channels 3 to 10 (sizes 60 to 200 μm) in this case, except that there were no particles of 180 μm size (channel 9). No particles larger than 200 μm were present. One particle was counted in each of channels 3, 4, 8, and 10; 3 in channel 5; 2 in 6; and 5 in 7. Thus, 14 particles were counted in the 1-sec interval ending at time 15:54:30 on this flight (1061).

Figure 8(b) shows the concentrations calculated when the counts in figure 8(a) are scaled for spectrometer sampling efficiency effects and airspeed as described in appendix C. This figure shows a concentration of 358 m^{-3} in channel 3, 192 in 4, 391 in 5, 191 in 6, 370 in 7, 64 in 8, none in 9, and 71 in channel 10. Thus, the total particle concentration for this interval is 1637 m^{-3}. Charging-patch current during

this instant was -0.608 μA, typical of a visible cirrus cloud penetration.

The probe/data system just described provides comprehensive data, over its effective size range, for evaluating the effects of cloud particles on LF under a range of operational conditions. As discussed previously, operational LFC transports of the future will probably require some type of onboard cloud-particle detection system to inform aircrews that ambient particle concentrations are not conducive to maintaining laminar flow. Although a probe such as the OAP-230X probe would undoubtedly be effective when connected to instrumentation for crew-warning purposes, such probes have their main application as scientific instruments providing spectrometric data and requiring regular calibration, and thus, they represent a considerable oversophistication for airline service. The spectrometer output would probably have to be handled by a microprocessor in order to provide go/no-go LFC feasibility indications, in order not to add appreciably to crew workload. A system comprising a probe and microprocessor could be built, but a simpler device giving a meaningful reading directly is desirable. The second cloud instrument—the charging-patch particle detector—was evaluated as an example of such a simpler device. This instrument is described next.

Charging-Patch Cloud Particle Detector

As an aircraft encounters atmospheric particles, whether aerosols, volcanic dust, raindrops, or ice crystals, its airframe becomes charged by a triboelectric (frictional) effect. A detailed description of the charging and discharging phenomena associated with aircraft is given in reference 26. Therein, it is shown that the charging-discharging phenomena are dependent upon several factors, which are summarized in table 1. The particle impact-charge dependence is a very complex phenomenon and is by no means completely described analytically; nevertheless, by electrically isolating part of the airframe as a "charging patch," the level of charging current on the patch may be monitored, and hopefully related to the ambient atmospheric particle environment. The use of charging patches has some precedence. Most notably, Stanford Research Institute (SRI) used a system based on the charging-patch technique on a USAF contract to perform precipitation measurements (ref. 27), and the technique has been used in research on aircraft electrification, both in the Soviet Union (ref. 26) and in France (ref. 28). The research in reference 28 found that the aircraft charge could be directly related to the ambient particle environment if external electric fields from cloud charge centers were not present; where such charge

centers are present, the aircraft charge state depends both on the externally applied field and on the particle impact-generated (triboelectric) charging. Research into the charging of aircraft by ice particles is continuing, mainly because the charging characteristics of aircraft with composite structures need to be understood (ref. 29). Also, the technique was used previously in laminar-flow research for the X-21 aircraft (refs. 4 and 30), where it was found that a charge indication was usually correlated with a loss of laminar flow. Langley has refined the charging-patch concept to the application reported here, mainly by increasing its sensitivity and using improved fabrication methods (ref. 31). More importantly, in the JetStar LEFT application, the charging patch is supported by the Knollenberg probe as a truth device. This two-instrument approach was used to determine the suitability of the charging patch as a stand-alone cloud particle detector for LFC aircraft application.

Figure 9 is a block diagram of the system as developed at Langley (ref. 31). The system consists of three major components: an aluminum charging patch isolated from the rest of the airplane by fiberglass cloth and silicon rubber sealant, a two-channel charge-rate amplifier, and a surge arrestor. A prototype charging-patch system was fabricated and test-flown in 1982 on the vertical stabilizer of the Langley F-106B storm hazards aircraft to prove the technique and develop optimum amplifier settings for cirrus cloud detection. The surge arrestor was originally needed for the F-106B application because the prime mission of that aircraft was to measure lightning strikes during thunderstorm penetrations. The F-106B patch consisted of a 6- by 36-in. sheet of 0.016-in. aluminum, contoured and bonded to the leading edge of the vertical stabilizer. The net frontal area of that patch was approximately 0.5 ft^2. The device was flown on several missions, and cirrus clouds—even thin ones—were reliably detected (fig. 10).

A similar charging patch was constructed for use in the JetStar LEFT program and installed on the leading edge of the JetStar pylon as shown in figure 6. In this case, the patch was bonded to a backing plate which was bolted to the pylon for easy removal. The JetStar patch is twice the size of that on the F-106B and thus has a net frontal area of approximately 1 ft^2. The electronics are the same as those for the F-106B aircraft, but only the high-sensitivity channel of data is used because thunderstorm clouds are avoided. (Note that the position of the Knollenberg probe on the fin is also shown in fig. 9.) Nevertheless, the surge arrestor is used here also. A similar charging patch was also flown on a vertical stabilizer of an

F-14 aircraft, in the NASA Variable Sweep Laminar Flow Experiment (ref. 15).

Data

LEFT Development History

Modifications to the JetStar to convert it to the LEFT configuration shown in figure 2, including installation of the needed LFC suction system, were completed in March 1984. Systems evaluation and performance flight testing of the suction and contamination-protection/anti-icing systems were completed in July 1984. Initial flight testing began that same month and involved the achievement of laminar flow both at design and off-design conditions, and also the determination of the effect of varying suction distributions on the laminar flow. The contamination-protection/anti-icing systems were also further evaluated. All flights in this initial phase were conducted in the DFRF area. This phase was completed in July 1984. More detail on this initial testing phase may be found in reference 32.

As to the instrumentation providing the cloud particle measurements which are the major subject of this paper, the charging patch was installed first and was operational near the end of 1983. The Knollenberg probe was installed in the summer of 1984. Thus, all missions from the autumn of 1984 through the end of flight testing on October 23, 1987, had both these instruments operational. The real proving phase in the JetStar LEFT Program was the simulated airline service (SAS) phase, begun during July 1985 and summarized in references 10, 11, and 12. Therein, the airplane was operated out of several airports throughout the continental United States, as shown in figure 11. This diversity of sites allowed operations under various meteorological and contaminant conditions. In SAS, the JetStar performed two or more flights daily, with each flight consisting of take-off, climb to cruise altitude, achievement of laminar flow for some minimum period (20 min is the minimum desirable), descent, landing, and inspection of the test articles. The condition of the test articles, as to possible insect remains or other evidence of contaminated suction surfaces, was fully documented after each flight. These simulated airline missions provided realistic operational experience, because the LFC systems were operated in a "hands-off" mode, to establish a maintenance and reliability data base. The suction distributions determined as most optimum from the systems evaluation and performance phase were used in this simulated airline service phase; they were set and not changed, in keeping with the hands-off mode of

operation. Of course, the state of the boundary layer was monitored by instrumentation, as described in appendix A, so that long-term changes in the performance of the system could be documented. Deployments of the JetStar in the SAS, to each of the sites shown in figure 11, were limited to 2 weeks or less.

The SAS phase comprised three deployments: (1) to Atlanta, Georgia, in July 1985 (13 flights); (2) to Pittsburgh, Pennsylvania, in September 1985 (26 flights); and (3) to Cleveland, Ohio, in February 1986 (23 flights). A chronological listing of SAS flights is given as table 2. The table lists flights by number, giving departure and destination locations, noting whether clouds were encountered during cruise conditions with the LFC systems turned on and stabilized, and also noting comments gleaned from the aircrew's flight logs. It is noted that there were 13 flights in the Atlanta deployment, but 3 of them had aircraft instrumentation system malfunctions; therefore, only 10 provided useful data. Also, several photographs of ambient cloud conditions were taken to aid in the interpretation of the cloud probe data; these are also noted in the table. (Two of these photographs were presented earlier in fig. 5.) The SAS phase terminated in February 1986. Further LETA research with the JetStar was conducted through October 1987, when the LEFT program concluded.

Choice of Data for Analysis

As described earlier, Knollenberg probe data were obtained from the summer of 1984 onward and the charging patch was operational from the end of 1983, in the pre-SAS series of flights. Both these systems were tested in cloud encounters on these early flights and found to perform well. These early tests showed that particles were being counted by the probe, and simultaneous charging of the patch was occurring. It was found that negative charging was experienced in ice clouds and positive in water clouds. Also, these early flights were useful in calibrating the charging patch by means of probe measurements, to derive ranges of current that are characteristic of clear air and unclear air (i.e., cloudy or hazy) conditions. In this connection, it was found that a charging-patch current between 0 and -0.05 μA was highly correlated with a particle-free environment, as shown by the Knollenberg probe. Preliminary probe and patch measurements from these early flights were given in reference 13. A more extensive set of results, based on analysis of a portion of the SAS missions and correlating LF percentages along with probe and patch measurements, was presented in reference 33.

From the total population of 62 SAS flights available, 19 flights were chosen for analysis. Figure 12

6

gives the rationale for the choice or rejection of a given flight. Key factors in the choice or rejection were aircrew notes (from flight logs) and a preview of LF percentages and charging-patch readings obtained from quick-look data stored on floppy disks. Most of the flight time at commercial airline altitudes takes place in clear air conditions; this was also true for the SAS missions. Although this result is favorable for obtaining laminar flow, for the purpose of this study, these are the "non-interesting" cases. Preference in this analysis was instead given to cloudy conditions, which affect LF and "exercise" the particle instrumentation. Therefore, flights where the aircrew noted penetration of cirrus and haze were given preference in the analysis. Therefore, the analyzed data indicated more cloud encounters, on a percentage basis, than would be derived from a complete survey of all flights. (This point is elaborated later.) Indeed, aircrew notes were the most important criterion in choosing a flight for analysis; the notes were extremely useful and of vital importance. Quick-look records, with temporal resolution of 2 to 3 min, indicated the behavior of LF and charging-patch readings during each flight. Where fluctuations of LF level and charging-patch current occurred, a given flight was analyzed further. Conversely, if LF remained at a high level and little charging-patch activity occurred, a flight was usually regarded as not interesting enough for analysis. Again, this procedure biases the results toward lower amounts of laminar flow overall than would be obtained in a complete survey of all the data. Figure 13 is an example of a quick-look data workup from an "interesting" flight. The changes in charging current, accompanied by changes in LF, are apparent. (Changes in Mach number are small for this example, and change in altitude is slight. The changes in LF occur concurrently with changes in charging-patch current. Note that LF returns to original values when current does.) When the selection process described was complete, portions of 19 flights (out of the total of 62), totalling 37 008 sec (10.28 hr) of data had been chosen. At the 1-sec data resolution, 37 008 data points were thus obtained. The 10.28 hr of data in the sample constitute approximately 26 percent of the total cruise time in the SAS program. The flights chosen for analysis are given in table 3, along with the time analyzed for each flight and aircrew notes on ambient cloud conditions.

Although this selection process may seem to have resulted in only cloudy or hazy data in the sample, in reality, most cloud encounters were transitory, and around 90 percent of all data were obtained in clear air. This is elaborated later. The 10.28 hr of data constitute a viable data sample. To process all

39.08 hr (ref. 10) of data was not necessary, since it contained very little additional cloud data.

Data Processing

Data from all JetStar LEFT flights were recorded on-board to computer-compatible tapes at 200 samples/sec data resolution. Later on, tapes for specific requested times of interest of the flights in table 2 were prepared by DFRF at 1 sample/sec resolution for subsequent analysis at Langley. Finally, data from these tapes were configured into formats compatible with the SPSS (Statistical Package for the Social Sciences, ref. 34) utility software. The SPSS software was used to analyze the data from each flight in several different ways. This analysis is described next.

Example of Concurrent Traces of Laminar-Flow Percentage, Particle Probe, and Charging-Patch Readings

Figure 14 shows an example of the concurrent time histories of laminar flow on the perforated and slotted articles, as calculated from pitot array measurements, and of the signals from the particle probe and charging-patch instruments. The data are taken from flight 1099, which was chosen for discussion because it is a particularly good example of a progression from flight in clear air to a cloud encounter back to clear air again. This was the flight for which the cloud photographs (fig. 5) were presented earlier. Figure 14 shows the areal extent of laminar flow on the three test articles as determined from pitot data (part (a)), the charging-patch current in microamperes (part (b)), and the total number of particles registered by the particle probe (not the concentration) during each 1-sec sampling interval (part (c)). The time traces begin at 9 hr 20 min 00 sec (0 sec in the figure) and extend 1000 sec or to 9 hr 36 min 40 sec. At the beginning of the trace, the perforated article is indicating 100 percent laminar flow, the charging-patch current is indicating a "clear air" reading of about -0.04 μA, and the particle count is zero. At about 750 sec, the percentage of laminar flow decreases precipitously as a cloud element is encountered. An immediate change in the charge level takes place at the same time, and particle counts are noticed, also. This first cloud encounter is temporary, however, and the laminar-flow readings return to near clear air values at about 800 sec. Thereafter, a more sustained encounter with thicker clouds begins at about 830 sec. Again, the results indicate a simultaneous loss of LF, an increase in charge current, and an increase in the number of particles. The lowest levels of LF are reached at about 860 to 880 sec (18 to 28 percent). At about 945 sec, the aircraft begins to exit the cloud, and charge and particle count

7

are starting to decrease. By about 990 sec, clear air is again encountered.

From figure 14, it is noted that the degree of LF on all articles changes simultaneously and that the particle count and charging-patch readings are related to the degree of laminar flow that is present. It is also noted that the charging patch generally responds slightly before the particle counter does, and the particle counter ceases responding before the charging patch does. This is because the charging patch responds to a wider range of particle sizes than does the particle counter and is also consistent with expected cloud particle distributions, in which smaller particles and lower particle concentrations surround denser concentrations and larger particles. From comparison of the three parts of the figure, it is also evident that particles smaller than 60 μm definitely affect laminar flow in addition to those 60 μm and larger in size.

Plots such as these were made for a large number of flights, and statistical analysis was performed, all of which led to the conclusion that both charging-patch and particle probe readings can be useful as reliable indicators of the loss of laminar flow. The loss of LF in clouds and haze is dramatically illustrated by figure 14. It is also apparent that the degree of LF achieved by the perforated LETA is consistently higher than that achieved on either surface of the slotted LETA and that the upper surface of the latter has a higher percentage than the lower. This relative ranking was observed in the vast majority of cases on all flights analyzed. In the analyses that follow, degree of LF is the dependent variable, and charging-patch current or particle concentration is the independent variable.

Analysis of Data

This investigation has two main goals: (1) to document thoroughly the effects of cloud and haze conditions on the LFC articles' performance and (2) to evaluate rigorously the performance of the cloud particle instrumentation in diagnosing conditions detrimental to laminar flow. To meet these goals, the following main analysis objectives were identified:

Document the degree of LF performance (i.e., the areal percentage of laminar flow, derived as described in appendix A) for all flights chosen for analysis

Measure the cloud particle environment on all flights simultaneously with the aircraft charging state

Correlate the areal percentage of laminar flow on both LETA's with the ambient particle concentration and with the aircraft charge

Use statistical techniques to identify significant effects and relationships

Evaluate the Knollenberg probe and charging patch as potential instruments for use on future LFC transports, on the basis of success, failure, and false-alarm probabilities

Secondary objectives were

Determine whether the LEFT data seem to follow the Hall criteria as described in appendix B

Obtain statistical data on the probability of encountering clear or unclear air in airline operations and compare with previous results (e.g., refs. 8 and 9)

Degree of LF Performance

Reference 33 reported on the degree of LF performance obtained during the first 11 of the 19 flights analyzed here. These 11 consisted only of the SAS missions out of Atlanta and Pittsburgh. Reference 33 reported that the average areal percentage of laminar flow for the perforated LETA was 92.3 percent. For the slotted LETA, the average was 73.9 percent for the upper surface and 69.6 percent for the lower surface. The relatively low performance of the slotted article is believed due to some deficiencies in the fabrication of the slotted LETA (refs. 10, 11, and 12) and not to any intrinsic lack of merit of the slotted concept versus the perforated concept. The defect in fabrication was such that, although the area of the upper surface of the slotted LETA was at least 30 percent laminar 96 percent of the time, in only 2.5 percent of cases was it more than 99 percent laminar. The respective results for the perforated LETA were 98 percent for >30 percent laminar, and 63 percent for >99 percent laminar. The comparison between the perforated LETA and the two surfaces of the slotted LETA for the first 11 flights is shown by a histogram plot in figure 15. The marked superiority of the perforated LETA is apparent. Not only was the percentage of LF > 99 percent in 63 percent of cases; it was between 95 and 99 percent in about 18 percent of the cases. Thus, in 81 percent of the cases, the percentage of LF was 95 or greater. For the slotted article, the percentage of LF was 95 or greater in only about 3 percent of cases for both the lower and the upper surfaces. Further inspection of figure 15 shows that for most cases the slotted LETA's LF was <80 percent for the upper surface and <70 percent for the lower surface. Median values of LF were ≈99 percent for perforated, ≈80 percent for slotted upper, and 74 percent for slotted lower. The average percentages of LF in clear air were 96.3 percent for perforated, 78 percent for slotted upper, and 73.5 percent for slotted lower. There is some evidence from the data that flight at

the highest altitudes and Mach numbers caused compressibility effects and some resultant loss of laminar flow. The data presented herein have not been corrected for this effect and, thus, the true clear air percentages may be a little higher than these values.

Because the slotted LETA gave only about 78 percent LF, even in clear conditions, it was decided that further study of the correlations of the degree of LF with particle concentration would not be useful for the slotted LETA. Therefore, for all analyses performed since reference 33 was published, only the perforated LETA has been studied, and only the performance of the perforated LETA will be reported in this investigation. Figure 16 is a histogram distribution of the percentage of LF for the perforated LETA only for all 19 flights analyzed from the SAS sample, whereas only 11 flights are reflected in figure 15. Again, it is noted that the 11-flight sample included flights from the Atlanta (ATL) and Pittsburgh (PIT) deployments; the 19-flight sample consisted of these flights plus additional flights from the Cleveland (CLE) deployment. The distributions of the percentage LF on the perforated article for the two figures are similar, however.

In figure 16, clear bars indicate clear conditions, and shaded bars represent cloudy or hazy conditions. Numbers atop the bars indicate the percentage of cases overall. For example, in the category >99 percent LF, 53.93 percent of cases overall were in this category. About 1 percent (0.9, actually) of cases overall had LF > 99 percent, despite the presence of haze or clouds. Thus, by inference, 53.93 − 0.90 = 53.03 percent of cases had LF > 99 percent and were associated with clear air. Looked at another way, in 53.03/53.93 or 98.33 percent of cases with >99 percent LF, clear air was present. As the degree of LF decreases, an increasing percentage of cases is found to be associated with unclear air. For instance, in the 95- to 99-percent LF category, 0.9/19.35 or 4.65 percent of cases are associated with unclear air. In the 80- to 90-percent category and below, the majority of cases are associated with unclear air. Below 30 percent, effectively all cases are associated with unclear air.

Definitions of Clear and Unclear Conditions as Determined by Instruments

The designations "clear" and "unclear" were determined as follows. First, there are separate clear definitions for the Knollenberg probe and for the charging patch. In this report, for the probe, *clear* is defined as a particle count of zero during the sampling interval. *Unclear* is any count greater than zero. *Haze* is defined arbitrarily as a particle concentration (appendix C) of between 0 and 1000 m^{-3}. *Cloud*

is defined as a particle concentration of 1000 m^{-3} or greater. While these designations were arbitrary, they were adopted by correlating probe observations with JetStar crew notes of hazy or cloudy conditions. These designations also are believed consistent with verbal notes and particle concentrations obtained in the USAF Cirrus Cloud Particle Distribution Studies (e.g., refs. 23 and 24). It should be stressed that clear and unclear here are instrument readings and not aircrew observations.

For the charging patch, as mentioned previously it was found in early JetStar missions that a charging-patch current (conventional current notation) of between 0 and −0.05 μA was correlated with visibly clear flight conditions and zero particle count. Therefore, currents in this range were defined as indicative of clear conditions. As is described later, no separate categorization of patch readings into haze and cloud categories was possible. Therefore, patch readings lying outside the clear category are considered just as unclear. It will be important to keep these definitions in mind in the analyses and instrument comparisons which follow.

Now that the necessary definitions have been made, it is possible to analyze further the type of data presented in figure 16. The data in figure 16 were based on data from clear and unclear conditions as determined by the charging-patch readings. It is interesting to consider how the data would appear were the distinction made on the basis of Knollenberg probe readings. A comparison is presented in table 4. Therein, the percentage of overall observations in clear and unclear categories, as determined by both probe and patch, is given along with the extent of LF (LF category). (The unclear probe readings comprise both cloud and haze situations.) Comparison of the totals in the clear category for the two instruments and for the unclear category shows that the probability of clear conditions, as detected by the patch, is less than that for the probe. The charging patch had 79.84 percent of cases overall as clear, whereas the probe had 91.71 percent. Conversely, the percentage of unclear observations from the patch was higher than that for the probe—20.16 and 8.29 percent, respectively. These results are not surprising because, as remarked previously, at our airspeed the patch responds to a wider range of particle sizes than does the probe. Based on the totals in table 4, it might appear that the probe is slightly superior to the patch, in discriminating clear and unclear conditions. However, when the results are related to the overall percentages of clear and unclear conditions, as determined by the two different instruments, a different interpretation, in terms of application to LFC aircraft, emerges. A relatively higher percentage of

aircraft, emerges. A relatively higher percentage of cases is associated with high LF percentages, when the charging-patch definition of clear is used than when the probe definition of clear is used. For example, 53.03 percent of cases, out of the 79.84 percent in the clear category, or 66.42 percent have a LF value of 99 percent or greater. With the probe data, a similar calculation yields only 53.63/91.71, or 58.48 percent. Similarly, if all cases with LF > 95 percent are considered, (53.03 + 18.45)/79.84, or 89.52 percent of cases are in this category with a patch clear reading, but only (53.63 + 19.24)/91.71 or 79.46 percent of cases with a probe clear reading. Further results such as these are presented with respect to cumulative frequencies (for definition, see ref. 34 or 35, e.g.) in table 5. From the table it is evident that a reading of clear with the patch is more likely to be associated with a high level of LF than is a reading of clear from the probe. However, a reading of unclear from the probe is *less* likely to be associated with a given high level of LF than is a reading of unclear from the patch. The relative influence of these results on the choice of an instrument for LFC transport application will be elaborated later in the section "Evaluation of Two Instruments as Diagnostic Indicators of Probable Loss of Laminar Flow."

Figure 17 shows a plot of the data in table 5. The curves here are cumulative distribution functions; the ordinate gives the probability of exceeding the percentage of laminar flow on the abscissa. The figure again makes the main point that the patch is superior for identifying clear air conditions and the probe is superior for identifying unclear conditions.

Figure 17 and the data in table 5 also show the marked difference in the probability of obtaining a high level of LF between clear and unclear conditions. For example, to obtain an areal percentage of laminar flow that is 90 percent or greater with the patch criterion for clear air, the probability is 0.9272. For unclear air, the probability is 0.1631. For the probe criteria, the respective values are 0.8372 and 0.0632. The data plotted in figure 17 represent overall values for the 19 flights in the sample. A flight-by-flight description of the average degree of LF overall for each flight and of the percentage of hazy or cloudy conditions for each flight is given next.

Laminar-Flow Performance on Each Flight

Table 6 is a listing for each flight, giving the range of altitudes flown, the number of data points (i.e., number of seconds of data at 1 sample per second) analyzed, and the overall average areal percentage of laminar flow during the data portion. All data were obtained during cruise conditions. The ambient cloud environment for each flight is also described by the percentage of time within clear air, haze, and clouds as determined by the Knollenberg probe reading. It is also described by the percentage of time with zero-range (i.e., charging-patch current between 0 and -0.05 μA) readings. Next, the average percentage of laminar flow is given for clear air, haze, cloud, and zero-range conditions. Overall averages for each quantity are given at the bottom of the table.

The overall average areal percentage of laminar flow was 83.50, with some missions having an average of more than 98. The low was 56.47, which was obtained during flight 1061, a very cloudy mission. Both the probe and patch indicated that only about 36 or 37 percent of the flight was flown in clear air. Faced with cloud cover such as this, an aircrew would undoubtedly seek a more cloud-free and LF favorable altitude or choose to fly with the LFC system shut off to save energy.

Overall, the Knollenberg probe indicated that 91.71 percent of the time was spent in clear air, 2.50 percent in haze, and 5.79 percent in clouds. The charging patch indicated zero-range conditions 79.63 percent of the time. Thus, there is about a 12-percent difference in the degree of cloudiness between the two measurements. However, both instruments indicate that clear air is the predominant condition.

When the average percentages of laminar flow in clear air, haze, and clouds are compared, the overall averages are, respectively, 92.55, 63.12, and 53.70. Thus, there is a marked decrease from clear air to haze, then another smaller decrease from haze to clouds. The clear air-haze difference is statistically significant as determined by the Scheffé one-way analysis of variance test (ref. 34) at the 95-percent confidence level; the haze-cloud decrease is not. The relative behavior just described existed on almost every flight, with flights 1085 and 1103 providing the only exceptions. (In these cases, there was higher LF in cloud than in haze.) The average zero-range reading was 95.92 percent and the average nonzero-range reading was 61.81 percent; this is a statistically significant difference as determined by the same test and confidence level. The zero-range reading is higher than the clear air reading, but usually not significantly so. Exceptions are noted on flights 1061, 1132, and 1136, where in each case the amount of LF obtained in clear air was considerably less than that obtained in zero-range conditions. It is believed that all these flights had concentrations of very small particles that were not detected by the Knollenberg probe but were sensed by the charging patch. As remarked previously, a zero-range reading is more indicative of a particle-free environment than a clear indication by the Knollenberg probe, because the probe only detects particles 60 μm in size or

greater at JetStar airspeeds. The difference between zero range and nonzero range was a marked one in nearly all cases; the closest agreement was on flight 1103, where the difference was only about 5 percent.

Because the degree of laminar flow seems directly proportional to the degree of clearness of the air, a regression analysis was performed to determine the degree of correlation of the average percentage of laminar flow with (1) the percentage of time in clear air and (2) the percentage of time in zero-range conditions. The results were

$$\overline{LF} = 51.89 + (0.4586 Z0) \quad (R = 0.907) \quad (1)$$

$$\overline{LF} = 37.06 + (0.5719 C0) \quad (R = 0.777) \quad (2)$$

where $\overline{LF}$ is the average percentage of laminar flow on the flight, Z0 is the percentage of time in zero-range conditions, C0 is the percentage of time in zero particle conditions, and R is the multiple correlation coefficient; an R value of 1.00 indicates perfect correlation and a value of 0 indicates no correlation (ref. 34). The square of R indicates the fraction of statistical variance that is explained by the regression equation. Thus, 0.823 (82.3 percent) of the variance in LF is explained by variability in Z, leaving 0.177 (17.7 percent) random error. For C0, only 60.4 percent of the variance is explained; 39.6 percent is random error. Thus, a good correlation exists for both equations, but the correlation with zero-range condition is the higher, 0.907. Equations (1) and (2) may be used to predict the average value of LF on a flight given, respectively, the percentage of zero-range conditions or particle-free (clear) conditions. For a Z0 value of 100 percent, $\overline{LF}$ would be maximized at 97.75 percent. For a C0 value of 100 percent, $\overline{LF}$ would be 94.25 percent. The 19-flight ensemble had an average Z0 of 79.84 percent, and an average C0 value of 92.55 percent. These values translate to expected overall average LF values of 88.50 and 89.99 percent, respectively, both of which are a little higher than the observed 83.50 percent value of LF.

Particle and Charge Conditions on Each Flight

Table 7 provides the particle concentration, in meter^{-3}, and the average, maximum, and minimum particle sizes in micrometers measured by the Knollenberg probe on each flight. A subcategorization by haze and cloud conditions is also given. (Clear air is, of course, not listed, because this category by definition contains no particles.) The table also includes values of the average, minimum, and maximum charging-patch current values in microamperes obtained in clear air, haze, and cloud conditions.

From inspection of table 7, it is noted that all flights except flights 1082, 1141, and 1153 encountered haze or cloud particle concentrations. Where haze was encountered, particle concentrations ranged from a minimum of 150 m^{-3} to the arbitrary maximum of 1000 m^{-3} (in the table, $1.5E2 = 1.5 \times 10^2 = 150$), with average concentrations of about 500 m^{-3}. In cloud conditions, the minimum concentrations ranged from the arbitrary lower limit of 1000 m^{-3} on most flights, to 1800 m^{-3} on flight 1085. Maximum concentrations were obtained on flights 1081 and 1099, at about 15 million to 16 million m^{-3}. The lowest in-cloud maximum was obtained on flight 1103, 3800 m^{-3}.

Particle sizes in both haze and clouds usually began near the minimum size (60 μm) measurable at these airspeeds. The average size of particles in haze seems larger than the average size of particles in clouds in most cases; this was also true of the maximum size. This situation most likely reflects fragmentation of larger haze particles in the cloud environment.

Statistical Study of Degree of LF Versus Particle Concentration and Charge Level

Study of the charging-patch currents in table 7 shows that the average current in clear air was generally near -0.01 μA, whereas the average values in haze and clouds varied considerably, all the way up to the electronics saturation values of ±1.33 μA. No clear pattern emerged from the data, as to a possible relation between current level and extent of laminar flow, although one was sought. This finding was not unexpected, because results of previous research have shown that a wide range of charge conditions can be obtained in clouds (refs. 26 to 28). The only clear conclusion gained in statistical significance testing was that high levels of LF were significantly related to charging-patch current readings being in or near the zero range. Again, the test used was the Scheffé one-way analysis of variance test at the 95-percent confidence level. Table 8 shows the basis for this conclusion. In the table, the average value of LF in each of 15 charging-patch current range categories is given for each flight. The current range was from -1.330 to more than 1.319 μA. For a finer-scale analysis, the zero range (-0.05 to 0 μA) was subdivided into two equal ranges. Inspection of table 8 shows that the highest average value of LF was achieved in the current range between -0.025 and 0 μA on every flight except on one (1141) where the peak was achieved in the 0 to 0.25 μA range. (On that flight, however, there were fewer than 5 samples in the 0 to 0.05 μA range.) The LF values in or near the zero range on most flights are significantly higher than the

LF values in the rest of the bins. The values in the rest of the bins are usually more similar, statistically, to each other.

Table 8 shows that the average LF values in the −0.025 to 0 μA and −0.05 to −0.025 μA bins are considerably different. Therefore, it might be thought that using a zero range of −0.025 to 0 μA would be associated with higher average values of LF than would the originally specified −0.05 to 0 μA range. This was checked out, and an improvement of between 0.01 and 0.02 was indeed obtained in the cumulative frequency values shown in table 4. For example, the fraction of observations having LF $\geq$ 99 percent rose from 0.6642 to 0.6780, the fraction having LF $\geq$ 95 percent rose from 0.8952 to 0.9128, and the fraction having LF $\geq$ 90 percent rose from 0.9272 to 0.9437. The reason that larger improvements were not seen is that the number of observations in the −0.025 to 0 μA bin was much larger than that in the −0.05 to −0.025 μA bin (28867 observations versus 679, respectively); therefore, the results for the overall −0.05 to 0 μA bins approximate those for the narrower −0.025 to 0 μA bin. The results indicate that the zero range can be narrowed, and some sensor performance sensitivity improvement obtained. This will be an advantage for more extensive chord laminarization in future LFC aircraft as discussed later.

The overall percentages of cases having given ranges of charging current are given in figure 18. The current was positive 16.51 percent and negative 83.50 percent of the time. Most of the negative contribution comes from the very slightly negative conditions occurring in conjunction with clear air, the 79.84 percent overall just discussed. Of this, 78 percent lies in the −0.025 to 0 μA bin, and 1.84 percent in the −0.05 to −0.025 μA bin. The remaining 3.66 percent comes from negative currents larger than −0.05 μA. The results obtained here are consistent with other investigations (refs. 26, 27, and 28) showing mostly negative currents at high tropospheric or stratospheric flight. The negative currents stem from ice-particle effects; the positive currents stem from water droplets (refs. 26 and 27). Due to the low temperatures at these altitudes, most particles consist of ice crystals.

Table 9 presents the results of another Scheffé test (95-percent confidence level) performed this time on particle concentration as measured by the Knollenberg probe. Once again, the highest average LF is found in the zero particle category in most of the cases. This bin usually has significantly higher LF than other bins; the other bins are not significantly different from each other. A steady falloff in LF is noted as particle concentration increases; the de-

crease is most marked as we go from clear air to haze but continues at a reduced rate thereafter. The decrease seems more monotonic here than is observed for the charging current in table 7; exceptions sometimes occur in cases with low sample size. As a rule, the LF values in the particle concentration bins seem less likely to be statistically different from each other than are the LF values in adjacent charging-current bins. Next, an evaluation of the patch and probe as diagnostic devices for use aboard LFC aircraft is given.

Evaluation of Two Instruments as Diagnostic Indicators of Probable Loss of Laminar Flow

Success Model

An evaluation was carried out of the performance of the Knollenberg probe and the charging patch in diagnosing the presence of LF-detrimental conditions. The first step in the evaluation process was the formulation of a success model, for determining what fraction of the time each instrument was successful in diagnosing such conditions, that is, the probability of success rate and, similarly, the probabilities of failure and false alarm. The success model was developed with the aid of the definitions given in table 10. In the table, the meteorological probabilities for clear air and unclear air are defined for each instrument as shown. Next, the conditional probabilities (ref. 35) are defined for L, an arbitrary level of LF. The choice of L would depend on the LFC application. In the examples that follow, it is assumed that a high level of L, namely 90 or 95 percent or more, would be desired; that is, an instrument that is sensitive to particle concentrations causing only 10 or 5 percent loss of LF is the type that should be designed. Success then has two component events: The level of LF must equal or exceed L when the instrument gives a clear indication and, to provide discrimination, the level of LF must be less than L when the instrument gives a not clear indication. The probability of each of these events is determined from the data. Then, the two probabilities are each multiplied by the respective meteorological (unconditional) probability and the sum is computed to yield the overall probability of success. Failure also has two component events. A failure occurs when the level of LF is smaller than L, despite a clear indication from the instrument, or the level of LF equals or exceeds L, despite an unclear indication from the instrument. The former type of failure is termed a "hard failure," in which LF is below expectation and aircraft economy suffers, despite a clear diagnosis from the

cloud instrument. The latter type of failure is termed a "false alarm," in which the level of LF remains higher than expected, although the cloud instrument indicates presence of clouds, and economy does not suffer. The overall probability of failure is computed in a manner similar to that described for the overall probability of success. Thus, the models for computing success, failure, and false-alarm probabilities for the two instruments have been defined. The actual evaluation for the 19-flight ensemble is presented next.

Results

Table 11 presents results of the success/hard-failure/false-alarm probability evaluation for the 19-flight ensemble of data. Results are presented for values of L between 0 and 99 percent; levels of 90, 95, and 99 percent were of prime interest because maintaining high levels of LF is the primary purpose of LFC flight. For $L = 99$ percent and using the charging patch as the diagnostic instrument, the probability of success is 0.729. The probability of hard failure is high, 0.262, but that for false alarm is only 0.009. If the criterion value of L is relaxed to 90 percent, the probability of success increases to 0.909 and that of hard failure is reduced dramatically to 0.058. The probability of false alarm is still only 0.033. The probability of success peaks at $L = 90$ percent and falls off both toward higher and lower values of L. As expected, the probability of hard failure decreases monotonically and the probability of false alarm increases as L is decreased.

Results using the Knollenberg probe as the diagnostic instrument show similar trends. The probability of hard failure decreases monotonically with decreasing L, equalling or exceeding the corresponding patch values at every value of L. The false-alarm probabilities increase monotonically with decreasing L and are lower than the corresponding patch values at every value of L. Success probabilities are lower than the corresponding values for the patch for $L = 70$ percent or higher. Peak success probability, 0.929, is reached at $L = 30$ percent.

Thus, the patch has significantly higher success probabilities than the probe for the prime LF values of interest and lower hard-failure probabilities, too. The probability of a false alarm for the patch is higher than that for the probe, but it is still relatively small. All these effects are explained by the patch's sensitivity to particles too small to be detected by the probe. When the probe indicates that particles are present, they indeed are present in more than sufficient number to affect LF. This is the reason that the probability of false alarm for the probe is lower than that for the patch.

In conclusion, both instruments show some success in discriminating conditions favorable and detrimental to maintaining laminar flow. The patch appears to give slightly better performance; this, coupled with its simplicity, ruggedness, and low cost, would make it the preferred candidate. The Knollenberg probe, however, would be required if knowledge of particle size is needed for research purposes. In the JetStar LEFT results, the Knollenberg probe data were extremely vital in establishing that the dynamic behavior of the charging current was due to the flux of atmospheric haze and cloud particles. The LEFT program has established that a charging patch can be used reliably as a stand-alone device. Appendix D gives more detail on the success analysis on a flight-by-flight basis.

Validation of Hall Criteria With JetStar Data

As previously mentioned, one of the goals of our investigation was to attempt to validate, with data from the LEFT program, the Hall criteria, which were originally developed to explain LF loss on the X-21 aircraft. The Hall criteria are described in appendix B. Figure 19 is a copy of the lower portion of the Hall criteria from figure B1, with an ordinate range change, and is overlaid with observations of particle concentrations and values of the concurrent degree of LF loss, computed as described earlier, for flight 1061. This flight was chosen because many clouds were encountered, and it had the largest range of particle concentrations experienced. Particle concentrations computed from the Knollenberg probe data were plotted for laminar-flow values lying in three arbitrarily chosen distinct ranges of LF on the perforated article: 25 to 35 percent, 75 to 85 percent, and greater than 85 percent. Several distinct sampling times were chosen at random for each of these ranges, so that 30 times were chosen overall.

Examination of figure 19 shows that the range of concentrations corresponding to the 25- to 35-percent LF range is considerably higher than that for the 75- to 85-percent range. Close examination of observations having LF values in the range 85 to 100 percent showed that for most cases no particles were observed at all; therefore, the preponderance of observations lay near the bottom of the figure, within Hall region 2 where it is predicted that LF will not be lost. However, there were some observations of high LF lying in Hall region 3, which is the region of partial LF loss. These observations are believed consistent, however, with the fact that a high but not 100-percent reading of LF over the leading-edge test article is very probably associated with a lower

overall chordwise percentage of LF, and the X-21 aircraft had LF on more of the chord than the JetStar ($\approx$60 versus 13 percent).

As cautioned earlier, only a limited degree of validation of the Hall criteria may be possible, because airfoil shape, altitude, and Mach number conditions are different from those for which the Hall figure was derived. Nevertheless, the data do seem to show "Hall criteria-like" behavior in that increasing particle concentrations do indeed seem to lead to progressively smaller degrees of laminar flow. Therefore, it is concluded that the Hall criteria seem to be consistent with JetStar observations and that the criteria are validated qualitatively.

Frequency of Cloud Encounters

As described earlier in table 4, the average percentage of clear air as determined from the Knollenberg probe measurements was 91.71 for the 19-flight ensemble. If charging-patch data are used, the value is 79.84. (See definitions of clear air in the section "Definitions of Clear and Unclear Conditions as Determined by Instruments.") Thus, the percentages of cases with unclear air were 8.29 as determined from probe data and 20.16 as determined from patch data. It is of interest to compare these results with earlier estimates. References 8 and 9 concluded that clouds or haze should be encountered about 6 percent of the time on average at LEFT altitudes. This estimate itself was consistent with an earlier Air Force estimate of 6 percent cited in reference 4. The data in references 8 and 9 were based on airborne particle sampling results and those in reference 4 on surface observations of visible cirrus cloudiness. Thus, the airborne probe measurements from these earlier sources (based on 6250 flight hours of data) seem in agreement with the reference 4 visual estimates of cirrus coverage. The LEFT figure of 8.29 percent is higher than the 6-percent value. Reasons for the increase are undoubtedly sample related. For, as remarked earlier in the section "Choice of Data for Analysis," a preference was given to flights reporting cloud encounters in order to evaluate the effects of clouds on LF and to evaluate the cloud instruments. *Therefore, many flights with no cloud encounters were not analyzed; this biases the result toward higher average cloudiness.* Viewed in this light, the 8.29-percent figure is probably not significantly different from the previous results.

The value of 20.16-percent nonclear conditions determined from patch data exceeds both the 8.29-percent and 6-percent estimates. This is due to the fact that the patch responds to small particles that the probe does not measure. These smaller particles do, however, contribute to charging and

also to some loss of LF. As remarked previously, the average percentage of LF, 83.50, lies between the probe clear air value of 91.71 and the patch clear air value of 79.84. Thus, it seems evident that these smaller subvisible particles are affecting LF to some extent.

Recommendations and Predictions for Future LFC Aircraft

Future LFC research aircraft will undoubtedly employ laminarization of much more than the 13 percent of chord used in the Leading-Edge Flight Test. An investigation such as just described here should also be carried out on such aircraft to determine the effects of clouds and haze on more extensive chord laminarizations (i.e., larger values of x/c) and to reevaluate the cloud detection instrumentation for application to such aircraft. If a Knollenberg probe-type instrument is flown, it should have the capability of sampling particles smaller than the 60-μm lower limit in this investigation. A charging patch identical to the one used here could be flown. With longer chord lengths, a better validation of the Hall criteria could be attempted. Photographs of cloud conditions will continue to be very useful in interpreting the data.

Predictions, based on projecting the current results to more extensive chord lengths, include

1. The average areal percentage of laminar flow will decrease because more of the area will be susceptible to contamination by turbulent areas near the leading edge.
2. The histograms and cumulative frequency distributions will have a greater uniformity than shown here.
3. The range of charging-patch currents coincident with maximum LF will be narrowed. The charging-patch instrument will be more sensitive; probability of success in diagnosing the LF condition should increase, and probabilities of hard failure and false alarm should decrease.

Concluding Remarks

An extensive data bank of concurrent measurements of laminar-flow areal extent, ambient atmospheric particle concentration, and aircraft charging state has been gathered for the first time during the LEFT (Leading-Edge Flight-Test) Program. From this data bank, 19 flights in the Simulated Airline Service (SAS) portion of the LEFT program have been analyzed to determine the effect of haze and clouds on laminar flow. A total of 10.28 hours of data (37 008 data points at 1-sec spacing) have been

analyzed, which represent approximately 26 percent of the available data. An extensive statistical analysis shows that there is a significant effect of cloud and haze particles on the extent of laminar flow (LF). The Hall laminar-flow loss criteria developed for the X-21 have been validated qualitatively by the JetStar LEFT results. Larger particles and higher particle concentrations have a more marked effect on LF than do small particles.

The Knollenberg probe and charging patch were both evaluated as diagnostic instruments for predicting the loss of LF and for application on LFC (laminar-flow control) aircraft. It was concluded that both these instruments are successful in this role. For a commercial LFC airplane, however, a charge patch would be preferred, due to its simplicity and sensitivity to small particles.

The results show that cloud-haze avoidance in LF aircraft operations must be a continuing goal to achieve maximum economic benefits of LF technology. Nevertheless, the results also show that the probability of cloud-haze encounter is small enough to make LF technology practical for everyday use.

Appendix A

Method of Calculating Areal Percentage of Laminar Flow

As shown in figure A1 for the left wing of the JetStar aircraft, viewed looking aft over the slotted test article in the foreground, an array ("rake") of 20 evenly spaced pitot tubes is mounted behind each leading-edge test article. These near-surface pitots are mounted with their axes about 0.060 in. off the surface. Also, there are 5 stations where two additional reference pitots are installed, at heights from the wing surface of 0.020 to 0.15 in., and two reference stations with the pitots about 2.0 in. above the surface. Figure A2 illustrates qualitatively how the pitot-tube readings are used to detect the nature of the boundary layer. The near-surface pitots measure the near-surface total pressure $p_{t,probe}$, and the reference pitots measure the reference pressure $p_{t,\infty}$. If laminar flow exists at the pitot tube, the boundary layer will be thin enough to pass under the tube, which will then register a pressure close to the reference pitot. But, if transition occurs ahead of the surface pitot tube, the tube will be immersed in a turbulent boundary layer with much reduced total pressure so that $p_{t,\infty} - p_{t,probe}$ is positive; the value of this pressure differential depends on where the transition occurs chordwise. A high pressure differential signifies that transition occurs near the leading edge; a lower value means that transition occurs farther along the chord. A relation of the chordwise

L-89-20
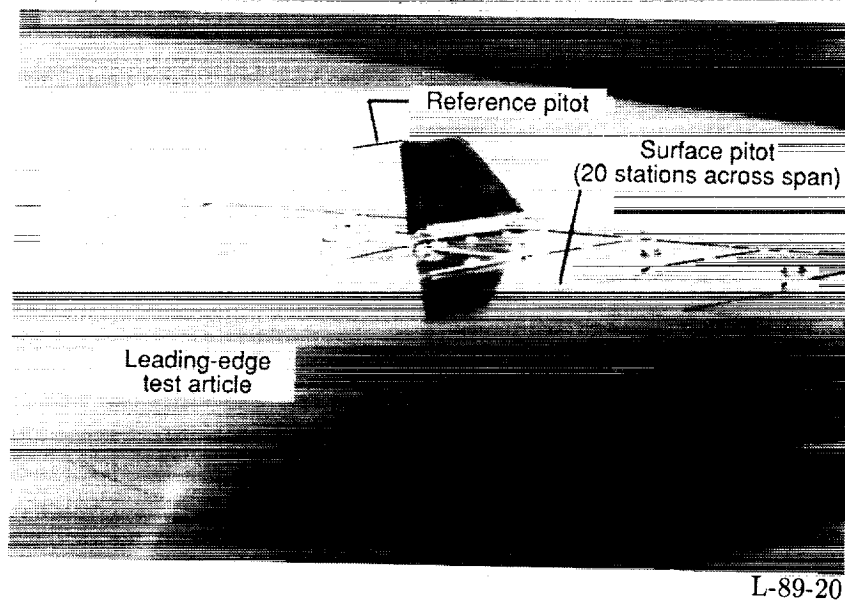
Figure A1. Pitot instrumentation for monitoring condition of boundary layer (on wing with slotted LETA).
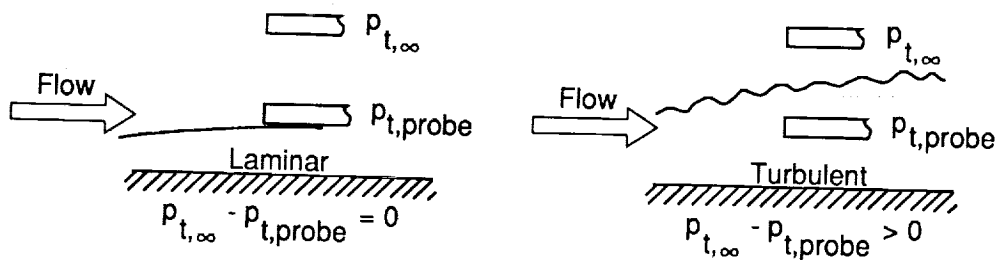
Figure A2. Determination of chordwise extent of LF at front spar.

16
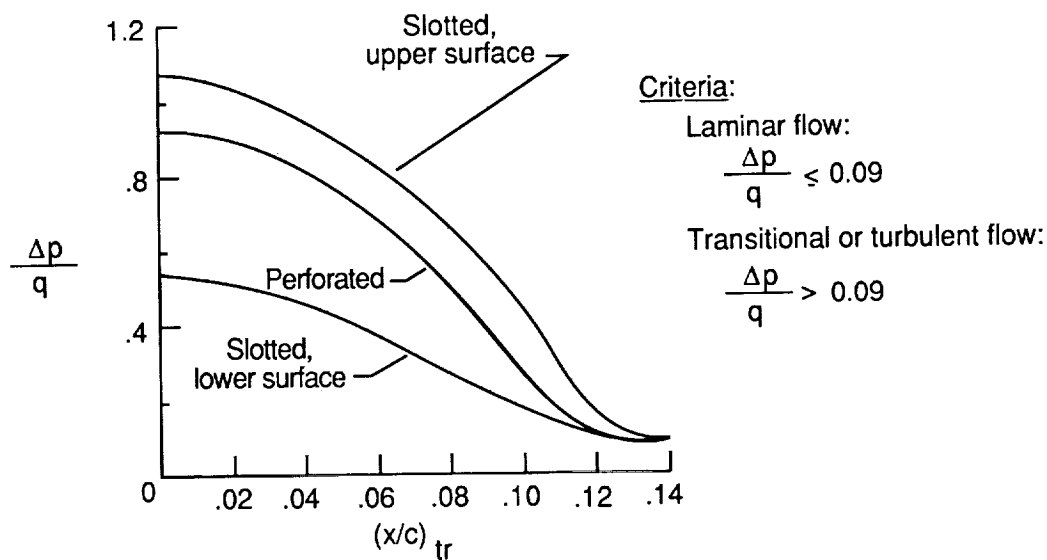
Figure A3. Computed chordwise extent of laminar flow at $M_\infty = 0.75$ and $h_p = 36\,000$ ft. $(x/c)_{tr,max} = 0.129$ for perforated LETA; $(x/c)_{tr,max} = 0.137$ for slotted LETA.
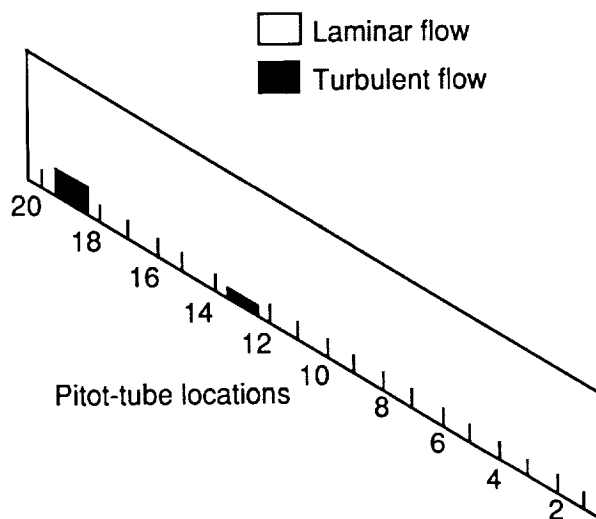
Figure A4. Example of calculation of areal extent of laminar and turbulent flow on perforated LETA. Flight 1059; Reynolds number per foot $= 1.521 \times 10^6$; % LF $= 98.63$; $M_\infty = 0.709$; $h_p = 36\,854$ ft; Charging-patch current $= -0.003$ μA.

location of flow transition and the pressure differential is shown in figure A3; this relation is based upon computation validated by measurements using a forced transition strip at the wing leading edge. Figure A3 shows the curves used for the perforated article and the upper and lower surfaces of the slotted article. These curves can only be considered as approximations, and the predicted transition locations are, hence, only approximate at best. Rigorously, the relationship is a function of several variables (e.g., altitude, angle of attack, Mach number, span station), but qualitative results are achievable with these simplified, one curve relationships. (The curves presented are for $M_\infty = 0.75$ and $h_p = 36\,000$ ft.) In figure A3, the ratio $\Delta p/q$ is the ordinate, where Δp is the measured pressure differential and q is the dynamic pressure. The abscissa is $(x/c)_{tr}$ or the fraction of chord at which transition takes place. Both leading-edge test articles extend to about 13 percent chord; the precise values are 0.137 for the slotted and 0.129 for the perforated article.

When the values of $\Delta p/q$ for all 20 near-surface pitots are calculated and allowance is made for the spanwise spacing of the pitots (i.e., area weighting), the total percentage area of the article that is laminar may be estimated. (The estimate is made by summing parallelogram areas as in figure A4. In the case of the slotted LETA, the end pitots, 1 and 20, lay outside the slotted portion of the article; therefore, readings from pitots 1 and 20 were disregarded in computing the areal percentage of LF—only readings from pitots 2 through 19 were used.) Figure A4 shows an example from a point in flight 1059 where it was calculated that 98.63 percent of the area of the perforated upper article had laminar flow. (The solid areas in the figure are turbulent.) In this paper, it is the areal percentage of laminar flow that is analyzed for changes with the ambient cloud particle concentration or charging-patch reading.

Appendix B

Hall Criteria for Loss of Laminar Flow on X-21 Aircraft

Hall's theoretical analysis, published in 1964 (ref. 19), considered only columnar ice crystals with a ratio of length to diameter of 2.5, because that crystal form was assumed to be the predominant one. When the theoretical impingement dynamics of this type of particle on an elliptical approximation of the forward portion of the X-21 airfoil was considered, the results indicated that, for $M_\infty = 0.75$ and $h_p = 40\,000$ ft, particles smaller than 4 μm in length will not impinge on the airfoil surface, but particles larger than about 50 μm will impinge at near free-stream velocity. If the particles are very small, that is, shorter than 4 μm, aerodynamic forces predominate over inertia forces, most particles follow streamlines, and few enter the boundary layer. As the ice particles become larger in size and more massive, they begin to penetrate the laminar boundary layer but do not cause a breakdown to turbulent flow until some critical size is attained. However, particles of this critical size must be present in a sufficiently large concentration in order to cause boundary-layer transition. Figure B1, from Hall's analysis, illustrates this discussion for flight conditions of $M_\infty = 0.75$ and $h_p = 40\,000$ ft. It should be noted that EMD is chosen as the abscissa variable on the figure. It has been found that ice particles in cirrus clouds occur in several crystalline forms and that the columnar variety is not necessarily the most numerous. (In any event, the regions on the figure pertain to columnar crystals.) According to the analysis, for columnar ice particles with an EMD larger than 33 μm, particle concentrations smaller than about 500 m^{-3} produce no effect on maintaining LF (region 2 of the figure). As particle concentrations increase above about 500 m^{-3} (for EMD greater than 33 μm), there is an increasingly detrimental effect on laminar flow (regions 3 and 4 of the figure).

It should be emphasized that the critical values of ice particle size and concentration level depicted in figure B1 pertain only to the X-21 aircraft, at $M_\infty = 0.75$ and $h_p = 40\,000$ ft. For a particular aircraft design, the critical values and the extent of the four regions just discussed are functions of airfoil leading-edge shape and sweep angle and of aircraft airspeed and altitude. The critical values and extent also depend on the particle shape. All these factors affect the number of ice particles penetrating the boundary layer.
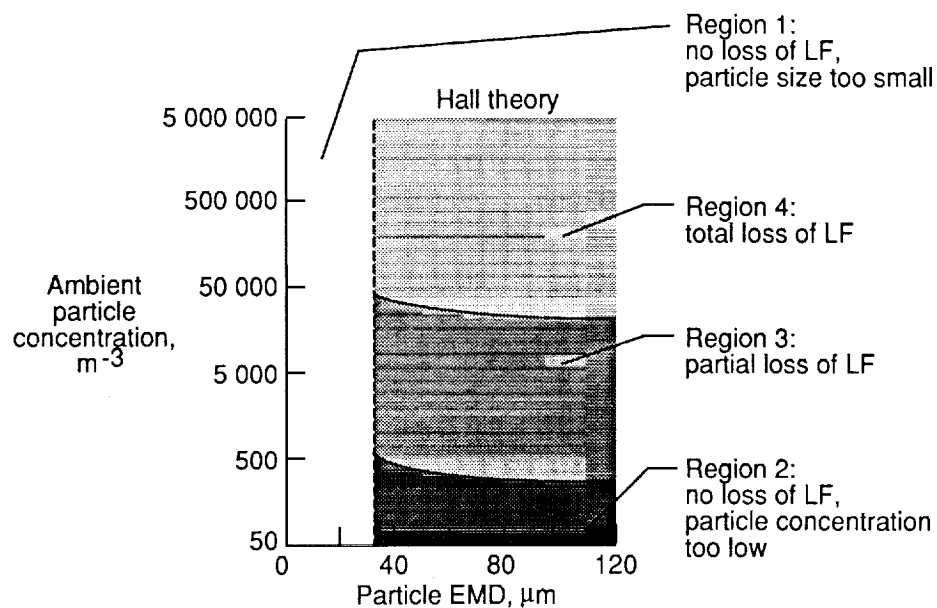

Figure B1. Predicted laminar-flow degradation in ice particle concentrations (Hall theory). Conditions for X-21 aircraft at $h_p = 40\,000$ and $M_\infty = 0.75$.

Appendix C

Knollenberg Probe Operation and Derivation of Particle Concentration From Probe Measurements

The purpose of this appendix is to present details relevant to understanding the measurement principle of the instrument and to deriving ambient particle concentrations from the instrument's measurements. (The electronics are not discussed here; for those, the reader is directed to the manufacturer's manuals. These manuals were used heavily in the description given here.)

The instrument used is a Particle Measuring Systems optical array cloud droplet spectrometer model OAP-230X designed for aircraft-borne operation. The instrument is a complete spectrometer probe; its output is particle size in binary code, accompanied by a strobe pulse to increment an appropriately addressed memory channel. Thus, the number of particles sensed by the probe in each of 30 size intervals (approximate size range 20 to 600 μm with 20-μm resolution) in a preset time interval may be measured. The principle of operation is shown in figure C1. The laser provides an illumination source. A particle is shown traversing the laser beam along the object plane. The particle's shadow is imaged by an optical system on a linear photodiode array lying in the image plane. The imaged shadow momentarily occults a number of optical array elements. In this case, the effective resolution of the array/optical system is 20 μm; therefore, particles are sized into 20-μm "bins." The electronics follow the particle's shadow as it travels along the image plane. Because the array is one-dimensional, only one dimension—the effective "crosswise width" of the particle—is sampled. (It is noted that two-dimensional PMS probes exist but they are considerably more expensive, and it was decided that they probably were not necessary for the JetStar LEFT application.) The particle size is determined by dividing the measured shadow size by the system's optical magnification. For this system, the magnification is 10.0. The laser used in the OAP-230X probe is a 1.5-mW He-Ne unit. The beam exiting from the laser is about 1 to 2 mm in diameter and is red in color. A condensing lens (fig. C2) is placed in front of the laser so that the beam is oval in the sampling area. When the optics are aligned correctly, this oval will have its long axis parallel to the photodiode array and its center in the middle of the array. After exiting the condensing lens, the beam is then deviated by a 45° mirror and traverses the area between the probe extension tips, as shown in figure C2. (Note that in the figure, the outline of the instrument shell is shown by a heavy line.)

The instrument is effective in detecting particles passing through a *sampling area* with vertical dimension D and horizontal dimension H, as shown in figure C3. Due to the finite width A of the sampling array, however, a *viewing volume DAH* (rather than a viewing area) is actually defined. From the movement of the aircraft a *sampled volume*, also shown in the figure, is defined. In the instrument, H is a maximum of 0.6 mm, A is 30 μm, and D is a maximum of
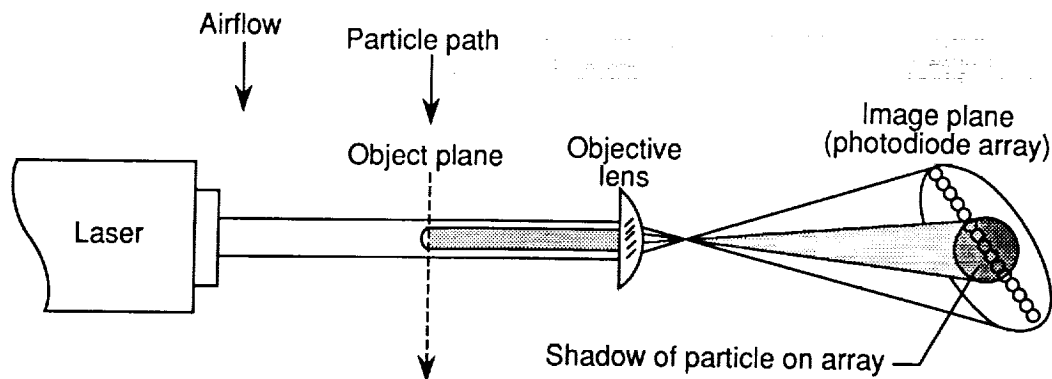
Figure C1. Principle of operation of Knollenberg probe.
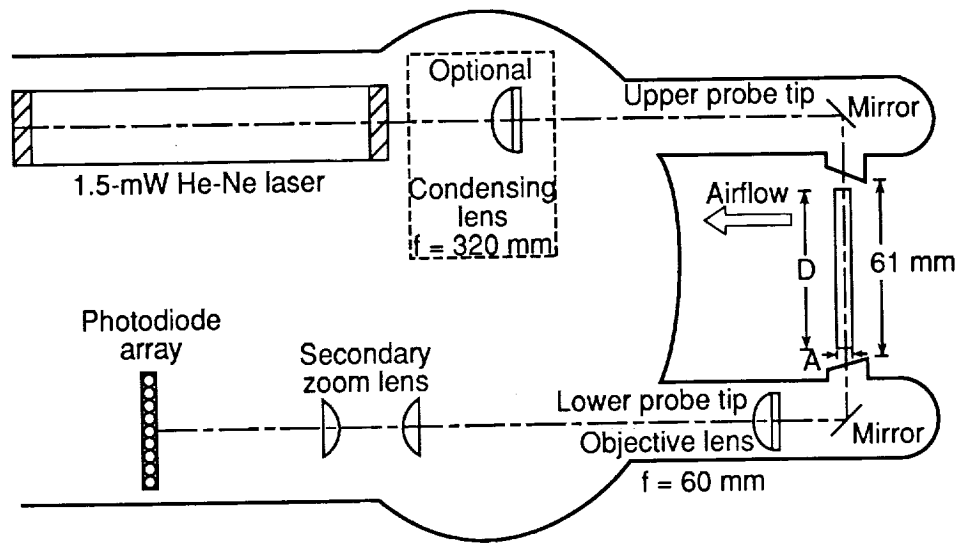
Figure C2. Optical arrangement of Knollenberg probe.
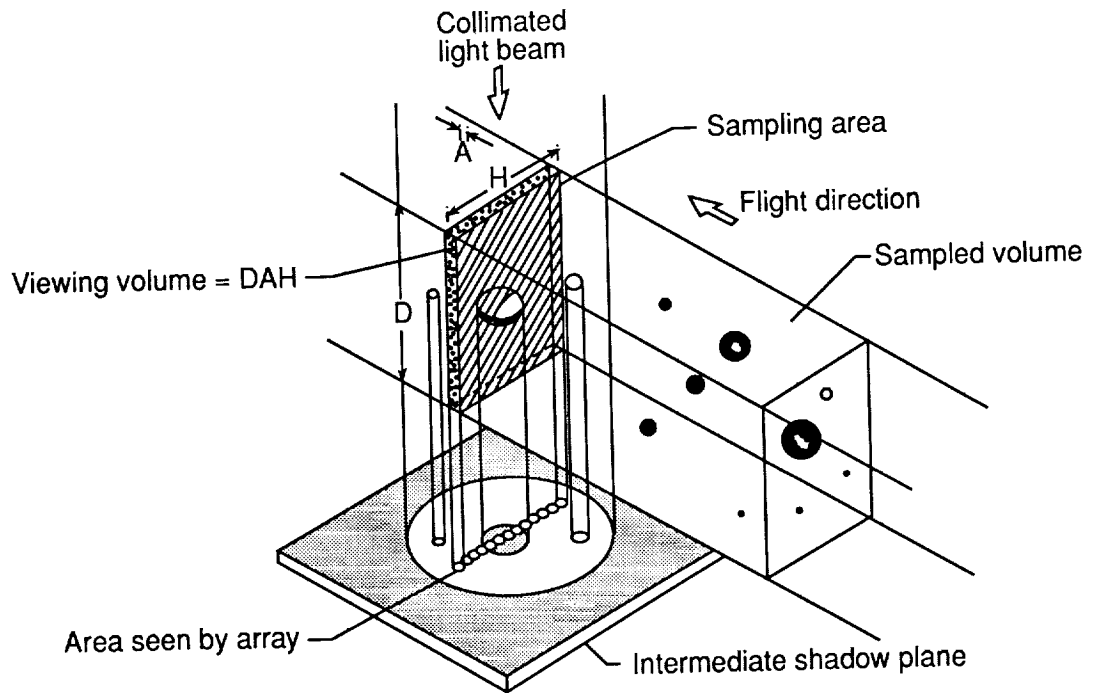
Figure C3. Imaging area and viewing volume for Knollenberg probe.

61 mm, the actual physical spacing of the probe tips. Thus A is a constant dimension, but D and H change with particle size, as is now explained.

The size of the aforementioned sampling area (shown shaded in fig. C3) depends on the size of the particle being sampled and is given by the following expression:

$$\text{Sampling area} = (10r^2) \, [N - (Y + 1)] \, \text{Resolution} \qquad \text{(C1)}$$

where

r	radius of particle, μm
N	total number of photodiodes used in OAP-230X probe, 32
Y	integer which describes number of photodiodes in array that are occulted by shadow of particle
Resolution	$= 20\ \mu$m

The $10r^2$ term determines the "depth of field," which is denoted by D in figures C2 and C3. This is the distance over which the probe can "see," correctly size, and accept a particle of a given diameter. For particles smaller than 156 μm, D is determined by optical and electronic considerations. All particles larger than 156 μm can be seen, so the upper limit on D for these particles is 61 mm, the actual physical spacing of the probe tips, as shown in figure C2. The term $N - (Y + 1)$ describes the effective array width. This is *not* equal to the dimension H in figure C3. Rather, it is a measure of the number of particles of a given size that could be counted meaningfully, side-by-side, within the dimension H. Considered in another way, it is the available change in position, for a particle of a given size, from the limit at one end of the photodiode array, just short of being rejected by one end element (number 1), to the other end of the photodiode array, just short of rejection by the other end element (number 32). (In this connection, it can be explained why the OAP-230X probe has 32 photodiodes, but counts in only 30 channels. This is because the two end diodes are used as reject indicators; that is, when either of these two end diodes is occulted, the measurement is rejected. In other words, the particle is not counted. In this way, only shadows lying fully within the array are measured and recorded. Thus, the effective array width eliminates from consideration any particle that could possibly be occulting either one or both of the end diodes.) Therefore, the sample *area* is the product of the effective array width and depth of field; the sample *volume* is this area times the aircraft velocity.

For completeness, a tabulation of the depth of field D, effective array width H, and actual sample area, taken from manufacturer's manuals, is given as table C1. It should be noted that an additional correction factor F recommended by PMS has been incorporated into the depth-of-field factor listed for the first three channels so that the depth of field is $F \times 10r^2$. For the first three channels, F equals 0.26, 0.62, and 0.89; for all other channels, F equals 1.0. The depth of field is smallest for the smallest particles, becoming larger until it becomes a constant 61 mm for particles larger than about 160 μm, but the effective array width is largest (0.6 mm) for the smallest particles, becoming smaller uniformly until it becomes 0.02 mm for the largest particles for the reasons noted previously. The result is that the actual sample area is largest for particles in the midrange and smallest at the ends.

Channel Sampling Effectiveness Factor F_Z

By knowing the effective sampling area for a given size particle from table C1 and the aircraft's true airspeed (TAS), $P_{Z,T}$, the number of particles sampled in a given time T in channel Z (the particle flux), can be converted to the ambient particle concentration C_Z by:

$$C_Z = \frac{\text{Number of particles of size } Z}{\text{Volume}}$$

$$= \frac{P_{Z,T}}{(\text{ASA})\,(\text{TAS})\,(T)} \tag{C2}$$

where C_Z is in meter^{-3} and ASA is obtained from table C1. With ASA in millimeter^2, TAS in knots, and elapsed time T in seconds, the relation becomes

$$C_Z = \frac{(1.9144 \times 10^6)\,P_{Z,T}}{(\text{ASA})\,(\text{TAS})\,(T)} \tag{C3}$$

When the factor 1.9144×10^6 and the actual sampling area are combined, a channel sampling effectiveness factor F_Z is derived, so that

$$C_Z = \frac{F_Z(P_{Z,T})}{(\text{TAS})\,(T)} \qquad \text{(C4)}$$

where F_Z is listed in table C2. It is noted that F_Z is smallest for the middle-size particles—those that are sampled most effectively after the optical, electronic, and effective array width constraints mentioned earlier are taken into account. For the lower sizes, the depth-of-field restriction would otherwise undercount particles; for the larger sizes, the rejection of particles occulting the end diodes would likewise result in an undercounting. Therefore, F_Z at both ends is higher than in the middle, to compensate for the undercounting.

Table C1. Sampling Area Chart for Knollenberg Probe

Channel	Actual range of diameters measured			Depth of field, D^a, mm	Effective array width, H^a, mm	Actual sample area, mm^2
	Low, μm	Average, μm	High, μm			
1	14.20	24.10	34.00	0.378	0.60	0.227
2	34.00	43.90	53.80	2.987	0.58	1.733
3	53.80	63.70	73.60	9.028	0.56	5.056
4	73.60	83.50	93.40	17.431	0.54	9.413
5	93.40	103.30	113.20	26.677	0.52	13.872
6	113.20	123.00	132.80	37.822	0.50	18.911
7	132.80	142.60	152.40	50.837	0.48	24.402
8	152.40	162.30	172.20	61.000	0.46	28.060
9	172.20	182.90	193.60		0.44	26.840
10	193.60	202.70	211.80		0.42	25.620
11	211.80	221.50	231.20		0.40	24.400
12	231.20	241.10	251.00		0.38	23.180
13	251.00	260.80	270.60		0.36	21.960
14	270.60	280.50	290.40		0.34	20.740
15	290.40	300.20	310.00		0.32	19.520
16	310.00	320.00	330.00		0.30	18.300
17	330.00	340.00	350.00		0.28	17.080
18	350.00	360.00	370.00		0.26	15.860
19	370.00	380.00	390.00		0.24	14.640
20	390.00	400.00	410.00		0.22	13.420
21	410.00	420.00	430.00		0.20	12.200
22	430.00	440.00	450.00		0.18	10.980
23	450.00	460.00	470.00		0.16	9.760
24	470.00	480.00	490.00		0.14	8.540
25	490.00	500.00	510.00		0.12	7.320
26	510.00	520.00	530.00		0.10	6.100
27	530.00	540.00	550.00		0.08	4.880
28	550.00	560.00	570.00		0.06	3.660
29	570.00	580.00	590.00		0.04	2.440
30	590.00	600.00	610.00	61.000	0.02	1.220

^{a}See figure C3 for definitions of D and H.

Table C2. Values of F_Z for 30 Channels of Knollenberg Probe

[For use in eq. (C4)]

Channel	F_Z, knot-sec-m^{-3}
1	8.4335E6
2	1.1047E6
3	3.7864E5
4	2.0338E5
5	1.3801E5
6	1.0123E5
7	7.8452E4
8	6.8225E4
9	7.1327E4
10	7.4723E4
11	7.8459E4
12	8.2588E4
13	8.7177E4
14	9.2305E4
15	9.8074E4
16	1.0461E5
17	1.1208E5
18	1.2071E5
19	1.3077E5
20	1.4265E5
21	1.5692E5
22	1.7435E5
23	1.9615E5
24	2.2417E5
25	2.6513E5
26	3.1384E5
27	3.9230E5
28	5.2306E5
29	7.8459E5
30	1.5692E6

Estimating Particle Count From Known Ambient Particle Concentration

If C_Z is known, then the number of particles to be counted in T seconds can be estimated.

$$P_{Z,T} = \frac{(C_Z)\,(\text{TAS})\,(T)}{F_Z} \tag{C5}$$

This expression is useful in determining whether the probe is operating correctly.

The factor F_Z was used to calculate C_Z for each channel. The results for all the channels were then summed to obtain the total particle concentration that was used in the statistical analyses in this paper.

Appendix D

Computation of Success, Failure, and False-Alarm Probabilities for the 19 Flights

The purpose of this appendix is to present in greater detail the success evaluation of the two particle detection instruments by presenting data for the 19 flights individually. Accordingly, tables D1 and D2 list the results for the charging patch and Knollenberg probe, respectively; the results pertain to a desired LF criterion value of 95 percent. In each table, the percentages of time in clear air and unclear air, as defined in table 10, are listed in columns ① and ②. The probabilities of meeting the 95-percent criterion in clear and unclear air are presented in columns ③ and ④, respectively. The probabilities of success, hard failure, and false alarm are presented in columns ⑤, ⑥, and ⑦. These probabilities, which were also defined in table 10, are related to the column listings here as follows (numbers in circles refer to column numbers in tables D1 and D2):

$$P(\text{Success}) = ③\left(\frac{①}{100}\right) + \left(1 - ④\right)\left(\frac{②}{100}\right) \qquad \text{(D1)}$$

$$P(\text{False alarm}) = ④\left(\frac{②}{100}\right) \qquad \text{(D2)}$$

$$P(\text{Hard failure}) = 1 - P(\text{Success}) - P(\text{False alarm}) \qquad \text{(D3)}$$

Comparison of the results in the two tables shows variability in the three probabilities and leads to the general conclusion that the probability of success is higher and the probability of failure is lower for the charging patch than for the probe. Out of the 19 flights, the patch had higher success on 14; the probe was superior on 4, and there was one tie. As to hard failure, the patch was superior (had a lower probability) in 12 cases, was inferior in 5, and was tied in 2 cases. In false alarm, the probe was superior in 10 cases, inferior in 7, and was tied in 1 case. Most of the relative success of the patch was achieved in the later flights, which were flown in winter during the Cleveland SAS deployment. This may have been due to relatively smaller particles occurring in the cold winter conditions—particles which affected charging but were not detected by the probe.

Table D1. Success, Failure, and False-Alarm Probabilities for the 19 Missions

[LF criterion, 95 percent; zero-range charging-patch reading of 0 to −0.05 μA defines clear air; ND indicates no data]

	(1)	(2)	(3)	(4)	(5)	(6)	(7)
Flight	% of time in clear air	% of time in unclear air	$P(\text{LF} \geq 95\%)$ in clear air	$P(\text{LF} \geq 95\%)$ in unclear air	$P(\text{Success})$	$P(\text{Hard failure})$	$P(\text{False alarm})$
1059	95.15	4.85	0.8605	0.0000	0.8673	0.1327	0.0000
1060	95.93	4.07	0.8796	0.0179	0.8838	0.1155	0.0007
1061	36.74	63.26	0.7002	0.0243	0.8745	0.1101	0.0154
1080	92.79	7.21	0.8858	0.0084	0.8934	0.1060	0.0006
1081	96.46	3.54	0.7057	0.0000	0.7161	0.2839	0.0000
1082	96.98	3.02	0.9955	0.0000	0.9956	0.0044	0.0000
1085	100.00	0.00	0.9510	0.0000	0.9510	0.0490	0.0000
1087	93.34	6.64	0.9840	0.0000	0.9849	0.0000	0.0000
1094	78.48	21.52	0.9686	0.0000	0.9754	0.0246	0.0000
1099	65.87	34.13	0.9485	0.1758	0.9060	0.0340	0.0600
1100	58.51	41.49	0.8490	0.1489	0.8498	0.0889	0.0618
1103	98.30	1.70	0.9575	0.5952	0.9481	0.0418	0.0101
1132	49.46	50.54	0.4644	0.0029	0.7336	0.2649	0.0015
1133	100.00	0.00	1.0000	ND	1.0000	0.0000	ND
1135	80.89	19.11	0.9996	0.3717	0.9286	0.0004	0.0710
1136	40.84	59.17	0.7237	0.0705	0.8455	0.1128	0.0417
1141	95.69	4.31	0.9754	0.0375	0.9748	0.0236	0.0016
1148	73.71	26.29	0.9880	0.0075	0.9892	0.0088	0.0020
1153	100.00	0.00	0.8614	0.0000	0.8614	0.1386	0.0000

Table D2. Computation of Success, Failure, and False-Alarm Probabilities for the 19 Missions

[LF criterion, 95 percent; particle count of zero defines clear air]

	(1)	(2)	(3)	(4)	(5)	(6)	(7)
Flight	% of time in clear air	% of time in unclear air	$P(\text{LF} \geq 95\%)$ in clear air	$P(\text{LF} \geq 95\%)$ in unclear air	$P(\text{Success})$	$P(\text{Hard failure})$	$P(\text{False alarm})$
1059	90.23	9.77	0.9039	0.0199	0.9113	0.0867	0.0019
1060	94.77	5.23	0.8887	0.0417	0.8923	0.1055	0.0022
1061	37.16	62.84	0.3077	0.0244	0.7274	0.2573	0.0153
1080	91.04	8.96	0.9895	0.0405	0.9049	0.0915	0.0036
1081	94.92	5.08	0.7155	0.0404	0.7279	0.2719	0.0002
1082	100.00	0.00	0.9654	0.0000	0.9654	0.0346	0.0000
1085	97.55	2.45	0.9534	0.8542	0.9336	0.0455	0.0209
1087	99.05	0.95	0.9466	0.4737	0.9426	0.0529	0.0045
1094	84.37	15.63	0.8980	0.0162	0.9114	0.0867	0.0025
1099	83.51	16.49	0.8106	0.1475	0.8340	0.1582	0.0078
1100	81.57	18.43	0.6755	0.1436	0.7273	0.2647	0.0080
1103	99.43	0.57	0.9511	1.0000	0.9457	0.0486	0.0057
1132	96.96	3.04	0.2384	0.0000	0.2616	0.7384	0.0000
1133	99.93	0.07	1.0000	1.0000	0.9993	0.0000	0.0001
1135	99.87	0.13	0.8808	0.0000	0.8810	0.1190	0.0000
1136	99.91	0.09	0.2057	0.0000	0.2064	0.7936	0.0000
1141	100.00	0.00	0.9192	0.0000	0.9192	0.0808	0.0000
1148	84.69	15.31	0.8651	0.0032	0.8853	0.1142	0.0005
1153	100.00	0.00	0.8614	0.0000	0.8614	0.1386	0.0000

References

1. James, Robert L., Jr.; and Maddalon, Dal V.: *Airframe Technology for Aircraft Energy Efficiency.* NASA TM-85749, 1984.

2. *Aircraft Operating Cost and Performance Report (For Aircraft Over 60 Seats)—For Calendar Years 1983 and 1984, Volume XIX.* Off. of Economics, Off. of the Assistant Secretary for Policy and International Affairs, U.S. Dep. of Transportation, Sept. 1985.

3. Wagner, Richard D.; and Fischer, Michael C.: Developments in the NASA Transport Aircraft Laminar Flow Program. AIAA-83-0090, Jan. 1983.

4. Whites, R. C.; Sudderth, R. W.; and Wheldon, W. G.: Laminar Flow Control on the X-21. *Astronaut. & Aeronaut.,* vol. 4, no. 7, July 1966, pp. 38–43.

5. Pfenninger, Werner; and Reed, Verlin D.: Laminar-Flow Research and Experiments. *Astronaut. & Aeronaut.,* vol. 4, no. 7, July 1966, pp. 44–50.

6. Povinelli, Frederick P.; Klineberg, John M.; and Kramer, James J.: Improving Aircraft Energy Efficiency. *Astronaut. & Aeronaut.,* vol. 14, no. 2, Feb. 1976, pp. 18–31.

7. Fischer, M. C.; Wright, A. S., Jr.; and Wagner, R. D.: A Flight Test of Laminar Flow Control Leading-Edge Systems. AIAA-83-2508, Oct. 1983.

8. Jasperson, William H.; Nastrom, Gregory D.; Davis, Richard E.; and Holdeman, James D.: *GASP Cloud- and Particle-Encounter Statistics, and Their Application to LFC Aircraft Studies—Volume II: Appendixes.* NASA TM-85835, 1984.

9. Jasperson, W. H.; Nastrom, G. D.; Davis, R. E.; and Holdeman, J. D.: GASP Cloud Encounter Statistics: Implications for Laminar Flow Control Flight. *J. Aircr.,* vol. 21, no. 11, Nov. 1984, pp. 851–857.

10. Maddalon, Dal V.; Fisher, David F.; Jennett, Lisa A.; and Fischer, Michael C.: Simulated Airline Service Experience With Laminar-Flow Control Leading-Edge Systems. *Research in Natural Laminar Flow and Laminar-Flow Control,* Jerry N. Hefner and Frances E. Sabo, compilers, NASA CP-2487, Part 1, 1987, pp. 195–218.

11. Wagner, R. D.; Maddalon, D. V.; and Fisher, D. F.: Laminar Flow Control Leading Edge Systems in Simulated Airline Service. Paper presented at the 16th Congress of the International Council of the Aeronautical Sciences (Jerusalem, Israel), Aug. 28–Sept. 2, 1988.

12. Wagner, R. D.; Maddalon, D. V.; Bartlett, D. W.; and Collier, F. S., Jr.: Fifty Years of Laminar Flow Flight Testing. SAE Tech. Paper Ser. 881393, Oct. 1988.

13. Davis, Richard E.; Fischer, Michael C.; Fisher, David F.; and Young, Ronald: Cloud Particle Effects on Laminar Flow in the NASA LEFT Program: Preliminary Results. AIAA-86-9811, Apr. 1986.

14. Braslow, Albert L.; and Fischer, Michael C.: Design Considerations for Application of Laminar Flow Control Systems to Transport Aircraft. *Aircraft Drag Prediction and Reduction,* AGARD-R-723, July 1985, pp. 4-1–4-27.

15. Maddalon, Dal V.; and Wagner, Richard D.: Operational Considerations for Laminar Flow Aircraft. *Laminar Flow Aircraft Certification,* Louis J. Williams, compiler, NASA CP-2413, 1986, pp. 247–266.

16. Etchberger, F. R.; et al.: *LFC Leading Edge Glove Flight—Aircraft Modification Design, Test Article Development, and Systems Integration.* NASA CR-172136, 1983.

17. Pearce, W. E.; McNay, D. E.; and Thelander, J. A.: *Laminar Flow Control Leading Edge Glove Flight Test Article Development.* NASA CR-172137, 1984.

18. Powell, Arthur G.: The Right Wing of the L.E.F.T. Airplane. *Research in Natural Laminar Flow and Laminar-Flow Control,* Jerry N. Hefner and Frances E. Sabo, compilers, NASA CP-2487, Part 1, 1987, pp. 141–161.

19. Hall, G. R.: *On the Mechanics of Transition Produced by Particles Passing Through an Initially Laminar Boundary Layer and the Estimated Effect on the LFC Performance of the X-21 Aircraft.* Northrop Corp., Oct. 1964.

20. Gardiner, B. A.; and Hallett, J.: Degradation of In-Cloud Forward Scattering Spectrometer Probe Measurements in the Presence of Ice Particles. *J. Atmos. & Ocean. Technol.,* vol. 2, no. 2, June 1985, pp. 171–180.

21. Dorsch, Robert G.; Brun, Rinaldo J.; and Gregg, John L.: *Impingement of Water Droplets on an Ellipsoid With Fineness Ratio 5 in Axisymmetric Flow.* NASA TN 3099, 1954.

22. Brun, Rinaldo J.; and Dorsch, Robert G.: *Impingement of Water Droplets on an Ellipsoid With Fineness Ratio 10 in Axisymmetric Flow.* NASA TN 3147, 1954.

23. Varley, D. J.: *Cirrus Particle Distribution Study, Part 1.* AFGL-TR-78-0192, U.S. Air Force, Aug. 7, 1978. (Available from DTIC as AD A061 485.)

24. Cohen, Ian D.: *Cirrus Particle Distribution Study, Part 8.* AFGL-TR-81-0316, U.S. Air Force, Oct. 28, 1981. (Available from DTIC as AD A118 715.)

25. Hobbs, Peter V.; and Deepak, Adarsh, eds.: *Clouds—Their Formation, Optical Properties, and Effects.* Academic Press, Inc., 1981.

26. Imyanitov, I. M.: *Aircraft Electrification in Clouds and Precipitation.* FTD-HC-23-544-70, U.S. Air Force, Apr. 1971. (Available from DTIC as AD 726 581.)

27. Tanner, R. L.; and Nanevicz, J. E.: *Precipitation Charging and Corona-Generated Interference in Aircraft.* AFCRL 336, U.S. Air Force, Apr. 1961.

28. Boulay, J. L.; and Laroche, P.: *Aircraft Potential Variations in Flight.* ONERA T.P. No. 1982-11, 1982.

29. Caranti, J.; and Illingworth, A. J.: Static Charging by Collisions With Ice Particles. *Proceedings International Aerospace Conference on Lightning and Static Electricity, Volume 2,* Culham Lab. (Abingdon, Oxon, England), 1982, pp. E2-1–E2-6.

30. Mee, Thomas R.: *An Investigation of Atmospheric Factors That May Affect Laminar Flow Control.* MR164, R212a, Meteorology Research, Inc., Dec. 1, 1964.

31. Campbell, Richard E.; and McPherson, John P.: Airborne Cloud Detector. *NASA Tech Briefs,* vol. 9, no. 2, Summer 1985, pp. 63–64.

32. Fisher, David F.; and Fischer, Michael C.: Development Flight Tests of JetStar LFC Leading-Edge Flight Test Experiment. *Research in Natural Laminar Flow and Laminar-Flow Control,* Jerry N. Hefner and Frances E. Sabo, compilers, NASA CP-2487, Part 1, 1987, pp. 117–140.

33. Davis, Richard E.; Maddalon, Dal V.; and Wagner, Richard D.: Performance of Laminar-Flow Leading-Edge Test Articles in Cloud Encounters. *Research in Natural Laminar Flow and Laminar-Flow Control,* Jerry N. Hefner and Frances E. Sabo, compilers, NASA CP-2487, Part 1, 1987, pp. 163–193.

34. Nie, Norman H.; Hull, C. Hadlai; Jenkins, Jean G.; Steinbrenner, Karin; and Bent, Dale H.: *SPSS—Statistical Package for the Social Sciences, Second ed.* McGraw-Hill, Inc., c.1970.

35. Hoel, Paul G.: *Introduction to Mathematical Statistics, Third ed.* John Wiley & Sons, Inc., 1965.

Table 1. Factors Important in Charging of Aircraft

Atmospheric medium	Aircraft characteristics	Flight regime
Particle phase (ice, water, or mixed) Particle shape Particle size Particle concentration Ambient electric field	Surface material (dural, composite) Airfoil shape Engine type (jet or prop) Static discharger effectiveness	Airspeed Altitude Power setting

Table 2. Listing of Simulated Airline Service Flights in LEFT Program

(a) Atlanta Deployment (13 Flights During July 1985)

| Flight | Date | From | To | Aircrew remarks | |
				Cloud encounter at cruise?	Other
1059	7/15	EDW	AMA	No	Cirrus, tops 31 500 ft
1060	7/15	AMA	BAD	Yes	
1061	7/15	BAD	ATL	Yes	In/out of clouds
1062	7/16	ATL	STL	No	LFC malfunction
1063	7/16	STL	ATL	No	
1064	7/17	ATL	CLE	Undetermined	Cirrus layer[a]
1065	7/17	CLE	SPI	No	
1066	7/17	SPI	ATL	No	
1067	7/18	ATL	MSY	No	Aircraft system malfunction
1068	7/18	MSY	ATL	No	Aircraft system malfunction
1069	7/20	ATL	ORF	No	
1070	7/20	ORF	ATL	No	
1071	7/22	ATL	LFI	No	

[a]Photograph taken by aircrew to aid in data analysis.

(b) Pittsburgh Deployment (26 Flights During September 1985)

| Flight | Date | From | To | Aircrew remarks | |
				Cloud encounter at cruise?	Other
1079	9/9	EDW	DEN	No	
1080	9/9	DEN	STL	Yes	Thin cirrus above aircraft
1081	9/9	STL	PIT	Undetermined	Small particles
1082	9/10	PIT	BOS	No	Clouds on descent
1083	9/10	BOS	PIT	No	
1084	9/11	PIT	ORD	Undetermined	Light, moderate turbulence[a]
1085	9/11	ORD	CHA	Yes	Particles[a]
1086	9/11	CHA	PIT	Undetermined	Turbulence[a]
1087	9/12	PIT	BNA	Yes	Hazy
1088	9/12	BNA	CLE	No	
1089	9/12	CLE	PIT	Yes	Thin cirrus[a]
1090	9/13	PIT	CHS	Undetermined	Turbulence[a]
1091	9/13	CHS	DCA	No	Jet stream turbulence
1092	9/13	DCA	PIT	Undetermined	(a)
1093	9/14	PIT	DET	No	
1094	9/14	DET	PIT	Yes	Thin cirrus[a]
1095	9/16	PIT	BGR	Undetermined	(a)
1096	9/16	BGR	JFK	No	(a)
1097	9/16	JKF	RDU	Yes	(a)
1098	9/16	RDU	PIT	No	(a)
1099	9/17	PIT	AZO	Yes	(a)
1100	9/17	AZO	PIT	Yes	Contrail, in/out cirrus
1101	9/18	PIT	STL	No	
1102	9/18	STL	OKC	No	
1103	9/18	OKC	ABQ	Yes	Between thunderstorms[a]
1104	9/18	ABQ	EDW	Yes	Cloud tops 25 000 ft

[a]Photograph taken by aircrew to aid in data analysis.

Table 2. Concluded

(c) Cleveland Deployment (23 Flights During February 1986)

Flight	Date	From	To	Aircrew remarks	
				Cloud encounter at cruise?	Other
1131	2/19	EDW	AMA	Yes	In/out cloud tops
1132	2/19	AMA	SPI	Yes	Thin cirrus
1133	2/19	SPI	CLE	No	Turbulence
1134	2/20	CLE	ATL	Undetermined	Scattered clouds
1135	2/20	ATL	ACY	Yes	Cirrus and haze
1136	2/20	ACY	CLE	Yes	Cirrus, haze, turbulence
1137	2/21	CLE	BOS	Yes	K.probe dirty
1138	2/22	BOS	CLE	Undetermined	
1139	2/24	CLE	TYS	Yes	Clouds on descent
1140	2/24	TYS	TPA	No	Ice on LETA's[a]
1141	2/24	TPA	BNA	Yes	Cirrus?
1142	2/24	BNA	CLE	Yes	Thin cirrus?
1143	2/25	CLE	GRB	No	
1144	2/25	GRB	LOU	No	
1145	2/25	LOU	CLE	No	
1146	2/26	CLE	BTV	Undetermined	
1147	2/26	BTV	LFI	No	
1148	2/26	LFI	CLE	Yes	Layers, tops 32 000 ft
1149	2/27	CLE	RIC	Yes	
1150	2/27	RIC	CLE	No	
1151	2/28	CLE	DSM	No	
1152	2/28	DSM	DEN	Undetermined	
1153	2/28	DEN	EDW	No	Thin cirrus?

[a] Therefore, data not analyzed.

Table 3. Listing of Simulated Airline Service (SAS) Flights Chosen for Analysis

Flight	Date	From	To	Aircrew remarks	
				Cloud encounter at cruise?	Other
(a) Atlanta Deployment (3 Flights During July 1985)					
1059	7/15	EDW	AMA	No	Cirrus, tops 31 500 ft
1060	7/15	AMA	BAD	Yes	
1061	7/15	BAD	ALT	Yes	In/out of clouds
(b) Pittsburgh Deployment (9 Flights During September 1985)					
1080	9/9	DEN	STL	Yes	Thin cirrus above aircraft
1081	9/9	STL	PIT	Undetermined	Small particles
1082	9/10	PIT	BOS	No	Clouds on descent
1085	9/11	ORD	CHA	Yes	Particles[a]
1087	9/12	PIT	BNA	Yes	Hazy
1094	9/14	DET	PIT	Yes	Thin cirrus
1099	9/17	PIT	AZO	Yes	(a)
1100	9/17	AZO	PIT	Yes	Contrail, in/out cirrus
1103	9/18	OKC	ABQ	Yes	Between thunderstorms[a]
(c) Cleveland Deployment (7 Flights During February 1986)					
1132	2/19	AMA	SPI	Yes	Thin cirrus
1133	2/19	SPI	CLE	No	Turbulence
1135	2/20	ATL	ACY	Yes	Cirrus and haze
1136	2/20	ACY	CLE	Yes	Cirrus, haze, turbulence
1141	2/24	TPA	BNA	Yes	Cirrus?
1148	2/26	LFI	CLE	Yes	Layers, tops 32 000 ft
1153	2/28	DEN	EDW	No	Thin cirrus?

[a]Photograph taken by aircrew to aid in data analysis.

Table 4. Distributions of Observations by Laminar-Flow Category, as Determined by
Charging Patch and Probe, Obtained in 19 Flights on Perforated LETA

LF category, percent	% of overall obs in category	Charging patch		Knollenberg probe	
		% of overall obs in clear category	% of overall obs in unclear category	% of overall obs in clear category	% of overall obs in unclear category
0	0.07	0.06	0.01	0.05	0.02
0–10	0.80	0.26	0.54	0.24	0.56
10–20	0.55	0.18	0.37	0.17	0.38
20–30	1.56	0.13	1.43	0.43	1.13
30–40	3.63	0.25	3.38	1.96	1.67
40–50	3.41	0.68	2.73	2.20	1.21
50–60	3.35	0.76	2.59	2.31	1.04
60–70	2.86	0.82	2.04	1.96	0.90
70–80	2.69	1.04	1.65	2.20	0.49
80–90	3.77	1.63	2.14	3.41	0.36
90–95	4.04	2.55	1.49	3.91	0.13
95–99	19.35	18.45	0.90	19.24	0.11
99–100	53.93	53.03	0.90	53.63	0.30
Total, % ...	100.01	79.84	20.17	91.71	8.30

Table 5. Cumulative Frequency Distributions of Areal Percentage of Laminar Flow for
Charging Patch and Probe, Obtained in 19 Flights on Perforated LETA

Areal percentage of LF, L	Fraction with $LF \geq L$, overall	Charging patch		Knollenberg probe	
		Fraction with $LF \geq L$, clear	Fraction with $LF \geq L$, unclear	Fraction with $LF \geq L$, clear	Fraction with $LF \geq L$, unclear
0	1.0000	1.0000	1.0000	1.0000	1.0000
10	0.9914	0.9962	0.9728	0.9969	0.9302
20	0.9859	0.9939	0.9546	0.9950	0.8846
30	0.9703	0.9922	0.8836	0.9903	0.7477
40	0.9340	0.9890	0.7162	0.9690	0.5459
50	0.8999	0.9804	0.5810	0.9450	0.3999
60	0.8664	0.9709	0.4526	0.9198	0.2744
70	0.8378	0.9606	0.3513	0.8984	0.1659
80	0.8109	0.9476	0.2694	0.8744	0.1066
90	0.7732	0.9272	0.1631	0.8372	0.0632
95	0.7328	0.8952	0.0894	0.7946	0.0476
99	0.5393	0.6642	0.0446	0.5848	0.0352

Table 6. Laminar-Flow Performance on the 19 SAS Flights Analyzed (Perforated LETA)

[ND indicates no data]

| Flight | Altitude, ft | Number of data points | Average LF, percent | Ambient environment, percent time in— | | | | Average LF percent, in— | | | | |
| | | | | K.probe | | | C.patch | K.probe | | | C.patch | |
				Clear air	Haze[a]	Clouds[b]	Zero range[c]	Clear air	Haze[a]	Clouds[b]	Zero range[c]	Nonzero range
ATL												
1059	36 700–36 900	1545	93.51	90.23	5.57	4.21	90.29	96.35	71.46	61.96	95.10	62.35
1060	32 600–36 800	1377	93.75	94.77	2.90	2.32	95.93	94.67	78.56	67.27	94.83	74.54
1061	28 700–32 900	1889	56.47	37.16	4.24	58.60	36.74	87.94	65.00	35.89	88.39	37.93
PIT												
1080	30 700–32 800	1651	91.42	91.04	3.82	5.15	92.79	95.86	55.88	39.19	95.10	44.04
1081	31 900–32 900	1948	89.07	94.92	1.13	4.16	96.46	91.72	44.98	38.00	90.76	43.05
1082	28 700–32 800	1821	97.96	100.00	0.00	0.00	96.98	97.96	ND	ND	99.69	42.15
1085	28 400–32 800	1958	96.74	97.55	0.77	1.73	100.00	96.87	82.38	95.67	96.74	ND
1087	32 500–37 800	2003	96.02	99.05	0.85	0.10	93.36	96.09	91.85	57.50	96.35	91.38
1094	30 800–32 800	1580	86.28	84.37	5.89	9.75	78.48	95.36	45.43	32.39	98.75	40.80
1099	25 700–34 800	1916	86.24	83.51	9.08	7.41	65.87	93.47	58.31	38.98	97.69	64.15
1100	20 800–36 800	1991	84.90	81.57	8.79	9.64	58.51	91.50	66.95	45.49	95.15	70.44
1103	25 600–34 900	2468	97.97	99.43	0.28	0.28	98.30	97.96	99.52	99.97	98.05	93.35
CLE												
1132	23 300–37 500	2699	73.01	96.96	2.52	0.52	49.46	74.21	35.24	33.86	86.23	60.09
1133	15 500–33 500	1439	98.63	99.93	0.17	0.00	100.00	98.96	98.63	ND	98.96	ND
1135	26 300–33 500	2999	95.42	99.87	0.13	0.00	80.89	95.50	34.37	ND	99.86	76.62
1136	23 100–39 400	2277	76.85	99.92	0.09	0.00	40.84	76.86	57.55	ND	96.53	63.25
1141	32 800–37 400	1857	96.03	100.00	0.00	0.00	95.69	96.03	ND	ND	98.14	49.27
1148	24 300–35 400	2031	87.61	84.69	3.70	11.52	73.71	94.84	52.66	46.03	99.74	53.63
1153	35 200–39 400	1559	98.53	100.00	0.00	0.00	100.00	98.53	ND	ND	98.53	ND
Overall av			83.50	91.71	2.50	5.79	79.63	92.55	63.12	53.70	95.92	61.81
Number of data points in sample		37 008		33 940	924	2144	29 471	33 940	924	2144	29 471	7537

[a] Particle concentration $< 1000 \text{ m}^{-3}$.
[b] Particle concentration $\geq 1000 \text{ m}^{-3}$.
[c] Charging-patch current between -0.05 and 0 μA.

Table 7. Particle and Charge Environment on the 19 SAS Flights Analyzed

[ND indicates no data]

Flight	Particle concentration, m^{-3}						Particle size, μm						Charging-patch current, μA								
	Haze			Cloud			Haze			Cloud			Clear air			Haze			Cloud		
	Max	Av	Min	Max	Av	Min	Max	Av	Min	Max	Av	Min	Max	Av	Min	Max	Av	Min	Max	Av	Min
ATL																					
1059	9.9E2	5.4E2	1.7E2	5.7E3	1.8E3	1.7E2	183	112	64	139	97	71	0	-0.01	-0.18	0	-0.04	-0.14	-0.01	-0.05	-0.11
1060	9.6E2	5.0E2	1.7E2	1.8E4	4.1E3	2.0E2	193	120	64	149	98	64	-0.01	-0.01	-0.11	-0.02	-0.05	-0.13	-0.02	-0.11	-0.35
1061	9.9E2	5.5E2	1.6E2	2.2E6	3.9E4	1.6E2	385	187	84	597	149	64	-0.01	-0.02	-0.43	1.32	-0.12	-1.15	1.32	0.81	-1.32
PIT																					
1080	9.9E2	5.0E2	1.5E2	2.9E4	5.2E3	1.7E2	203	103	64	172	110	64	0.07	-0.01	-0.48	0.11	-0.02	-0.40	0.68	0.02	-0.17
1081	8.5E2	4.9E2	1.5E2	1.5E7	2.0E5	2.0E2	244	132	64	444	115	64	0.04	-0.01	-0.05	0.06	-0.02	-0.13	0.39	-0.05	-0.17
1082	ND	ND	ND	ND	ND	ND	ND	ND	ND	ND	ND	ND	0.69	0	-0.02	ND	ND	ND	ND	ND	ND
1085	8.5E2	5.1E2	1.7E2	1.7E5	1.1E4	1.7E2	320	120	64	156	80	64	-0.01	-0.01	-0.03	0.01	-0.02	-0.02	-0.01	-0.02	-0.02
1087	9.3E2	5.1E2	1.8E2	1.3E5	6.6E4	1.8E2	143	98	64	84	81	78	0.06	-0.01	-0.02	0.06	0.01	-0.02	-0.01	-0.01	-0.01
1094	9.9E2	5.3E2	1.5E2	8.9E3	2.9E3	1.5E2	222	110	64	187	105	64	0.42	-0.01	-0.02	0.97	0.14	-0.02	1.32	0.39	-0.02
1099	9.9E2	4.2E2	1.5E2	1.6E7	1.2E5	1.5E2	274	135	64	444	103	64	1.32	0.04	-0.02	1.32	0.47	-0.01	1.32	0.84	-0.01
1100	1.0E3	4.7E2	1.5E2	1.7E4	3.7E3	1.5E2	261	121	64	149	100	64	1.32	0.06	-0.02	1.32	0.48	-0.01	1.32	1.02	0
1103	9.5E2	7.1E2	1.8E2	3.8E3	2.4E3	1.2E3	203	89	64	89	71	64	1.00	-0.01	-0.11	0.02	-0.02	-0.03	-0.01	-0.03	-0.03
CLE																					
1132	8.9E2	6.9E2	1.7E2	4.4E3	1.9E3	1.3E3	203	76	64	70	66	64	0.95	-0.01	-0.28	1.32	0.39	-0.04	1.32	0.51	0.03
1133	2.0E2	2.0E2	2.0E2	ND	ND	ND	203	203	203	ND	ND	ND	-0.01	-0.01	-0.01	-0.01	-0.01	-0.01	ND	ND	ND
1135	8.8E2	6.7E2	4.6E2	ND	ND	ND	84	74	64	ND	ND	ND	1.32	0.05	-0.02	1.32	1.32	1.32	ND	ND	ND
1136	1.0E3	2.6E2	1.5E2	ND	ND	ND	203	183	162	ND	ND	ND	1.32	0.36	-0.02	1.32	1.32	1.32	ND	ND	ND
1141	ND	ND	ND	ND	ND	ND	ND	ND	ND	ND	ND	ND	0.03	-0.01	0.58	ND	ND	ND	ND	ND	ND
1148	9.9E2	7.0E2	1.5E2	4.6E4	4.0E3	1.0E3	203	87	64	120	77	64	1.32	0.03	-0.24	1.32	0.078	-0.01	1.32	1.18	-0.13
1153	ND	ND	ND	ND	ND	ND	ND	ND	ND	ND	ND	ND	0	0	-0.01	ND	ND	ND	ND	ND	ND

Table 8. Average Percentage of Laminar Flow in Charging-Patch Current Range for Each of the 19 Flights Analyzed for Perforated Article

[ND indicates no data]

Flight	Average percentage LF in charging-patch current range, μA, of—														
	≤ -1.33	-1.33 to -1.0	-1.0 to -0.75	-0.75 to -0.50	-0.50 to -0.25	-0.25 to -0.10	-0.10 to -0.05	-0.05 to -0.025	-0.025 to 0	0 to 0.025	0.025 to 0.05	0.05 to 0.50	0.50 to 1.0	1.0 to 1.319	≥ 1.319
1059	ND	ND	ND	ND	ND	58.42	64.26	73.64	96.25	ND	ND	ND	ND	ND	ND
1060	ND	ND	ND	ND	a46.51	61.35	75.61	82.14	94.83	ND	ND	ND	ND	ND	ND
1061	ND	48.18	48.63	43.54	55.39	62.47	73.68	67.04	89.46	ND	ND	ND	ND	ND	32.07
1080	ND	ND	ND	ND	a48.44	a45.25	52.10	57.07	96.81	42.83	38.53	ND	b25.34	ND	ND
1081	ND	ND	ND	ND	ND	a28.75	a18.05	24.71	91.15	58.26	45.58	38.25	ND	ND	ND
1082	ND	ND	ND	ND	ND	ND	ND	ND	99.70	b82.97	59.23	41.01	38.25	ND	ND
1085	All observations were in zero range								99.70	All observations were in zero range					
1087	ND	ND	ND	ND	ND	ND	ND	ND	96.35	93.47	83.98	a80.68	ND	ND	ND
1094	ND	ND	ND	ND	ND	ND	ND	ND	98.75	66.29	54.48	37.20	27.30	21.59	a24.12
1099	ND	ND	ND	ND	ND	ND	ND	ND	97.68	94.94	86.48	61.94	40.35	35.93	41.47
1100	ND	ND	ND	ND	ND	ND	ND	ND	95.15	92.64	86.95	77.13	59.01	48.63	38.74
1103	ND	ND	ND	ND	ND	ND	b99.65	70.18	99.80	97.44	a91.19	89.97	b97.37	b65.10	ND
1132	ND	ND	ND	ND	a74.41	70.12	68.75	75.62	89.08	66.91	61.33	42.06	28.62	a26.32	a21.68
1133	All observations were in zero range								98.96	All observations were in zero range					
1135	ND	ND	ND	ND	ND	ND	ND	ND	99.86	98.79	93.78	75.68	47.61	42.89	36.62
1136	ND	ND	ND	ND	ND	ND	ND	ND	96.53	90.98	90.22	82.84	47.28	42.63	41.93
1141	ND	ND	ND	a41.91	45.13	46.32	48.27	55.72	98.87	a99.04	b100.00	ND	ND	ND	ND
1148	ND	ND	ND	ND	ND	64.82	83.52	87.52	99.81	83.08	81.54	55.45	45.85	53.03	48.21
1153	All observations were in zero range								97.65	All observations were in zero range					

a ≤ 5 observations in set.

b Only one observation in set.

Table 9. Average Percentage of Laminar Flow in Ambient Particle Concentration Range for Each of the 19 Flights Analyzed for Perforated Article

[ND indicates no data]

Flight	Average percentage of LF in ambient particle concentration range, m^{-3}, of—									
	0	100–250	250–500	500–1000	1000–2500	2500–5000	5000–7500	7500–10K	10K–25K	>25K
1059	96.35	75.42	73.66	67.89	62.85	56.87	57.68	ND	ND	ND
1060	94.67	76.36	81.07	78.37	76.90	66.84	[a]56.86	[a]47.45	[a]37.04	
1061	87.94	72.96	77.66	58.11	49.55	39.33	34.13	33.93	32.21	32.13
1080	95.86	75.09	52.63	53.93	47.07	37.61	32.15	27.92	24.86	[a]20.75
1081	91.72	[a]58.89	45.80	36.53	42.84	37.53	32.82	[a]31.84	28.38	[a]55.61
1082	97.96	No particles detected on this flight								
1085	96.87	76.25	[a]77.02	90.92	90.70	100.00	[a]100.00	[a]93.70	[a]100.00	[a]100.00
1087	96.09	95.45	93.99	86.70	100.00	ND	ND	ND	ND	[b]15.00
1094	95.36	49.93	40.90	46.34	34.66	32.13	24.55	[a]23.56	30.25	[b]99.84
1099	93.47	60.87	60.01	53.16	45.83	36.16	34.20	33.85	30.67	ND
1100	91.49	73.53	70.11	59.17	55.00	41.51	34.50	28.23	ND	ND
1103	97.96	[b]98.34	[b]99.88	99.69	99.95	100.00	ND	ND	ND	
1132	74.21	[a]36.10	34.03	35.83	35.41	[a]24.54	ND	ND	ND	ND
1133	98.96	[b]98.62	ND	ND	ND	ND	ND	ND	ND	ND
1135	95.50	ND	33.59	35.15	ND	ND	ND	ND	ND	ND
1136	76.86	[a]57.54	ND	ND	ND	ND	ND	ND	ND	ND
1141	96.03	No particles detected on this flight								
1148	94.84	60.06	59.09	50.30	48.99	45.11	41.45	40.59	45.15	[b]60.53
1153	97.65	No particles detected on this flight								

[a] ≤ 5 observations in set.
[b] Only one observation in set.

37

Table 10. Definitions of Probabilities (P) for Success Model

Particle environment:

$P(\text{CA}) \equiv P(\text{Clear air})$ $= P(\text{Charging-patch current in zero range}^a)$

$= P(\text{Knollenberg probe particle count} = 0)$

$P(\overline{\text{CA}}) \equiv P(\text{Unclear air})$ $= P(\text{Charging-patch current } not \text{ in zero range}^a)$

$= P(\text{Knollenberg probe particle count} > 0)$

$= 1 - P(\text{CA})$

Conditional probabilities:

$P_L(\text{S}|\text{CA}) \equiv P_L(\text{Success}|\text{Clear air}) = P(\text{LF} \geq \text{L}|\text{Clear air})$

$P_L(\text{S}|\overline{\text{CA}}) \equiv P_L(\text{Success}|\text{Unclear air}) = P(\text{LF} < \text{L}|\text{Unclear air})$

$P_L(\text{F}|\text{CA}) \equiv P_L(\text{Failure}|\text{Clear air}) = P(\text{LF} < \text{L}|\text{Clear air}) = 1 - P_L(\text{S}|\text{CA}) = P(\text{Hard failure})$

$P_L(\text{F}|\overline{\text{CA}}) \equiv P_L(\text{Failure}|\text{Unclear air}) = P(\text{LF} \geq \text{L}|\text{Unclear air}) = 1 - P_L(\text{S}|\overline{\text{CA}}) = P(\text{False alarm})$

Overall success or failure model:

$P_L(\text{S}) = P_L(\text{Success}) = P_L(\text{S}|\text{CA})\,P(\text{CA}) + P_L(\text{S}|\overline{\text{CA}})\,P(\overline{\text{CA}})$

$P_L(\text{F}) = P_L(\text{Failure}) = P_L(\text{F}|\text{CA})\,P(\text{CA}) + P_L(\text{F}|\overline{\text{CA}})\,P(\overline{\text{CA}}) = 1 - P_L(\text{S})$

[a]Between 0 and -0.05 μA.

Table 11. Diagnostic Indicator Evaluation Results

Level of LF performance on perforated LETA, L, percent	Charging patch			Knollenberg probe		
	P(Success)	P(Hard failure)	P(False alarm)	P(Success)	P(Hard failure)	P(False alarm)
0	0.798	0.000	0.202	0.917	0.000	0.083
10	0.801	0.003	0.196	0.920	0.003	0.077
20	0.803	0.005	0.192	0.922	0.005	0.073
30	0.816	0.006	0.178	[a]0.929	0.009	0.062
40	0.847	0.009	0.144	0.926	0.028	0.045
50	0.867	0.016	0.117	0.916	0.051	0.033
60	0.886	0.023	0.091	0.904	0.074	0.023
70	0.898	0.024	0.078	0.893	0.093	0.014
80	0.904	0.042	0.054	0.876	0.115	0.009
[b]90	[a]0.909	0.058	0.033	0.845	0.145	0.005
[b]95	0.898	0.084	0.018	0.808	0.188	0.004
[b]99	0.729	0.262	0.009	0.616	0.380	0.004

[a]Maximum success value.
[b]Level of prime interest.
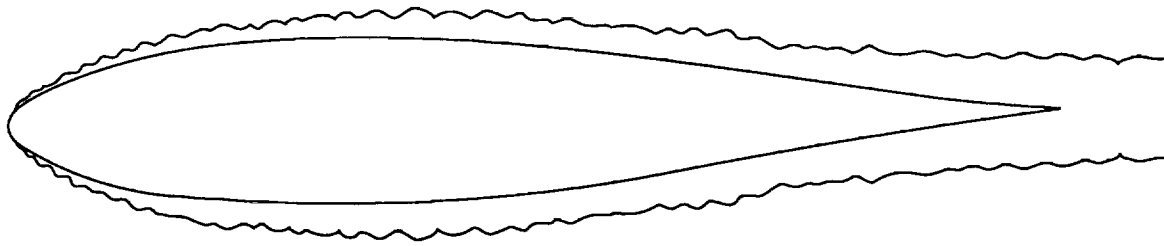
(a) Normal boundary layer (thick and turbulent with high drag).
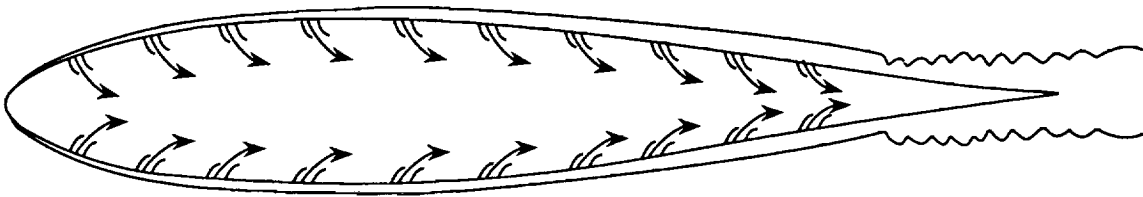
(b) Suction with stabilized boundary layer (thin and laminar with low drag).

Figure 1. Concept of suction-stabilized laminar flow.

Slotted LETA

Perforated LETA
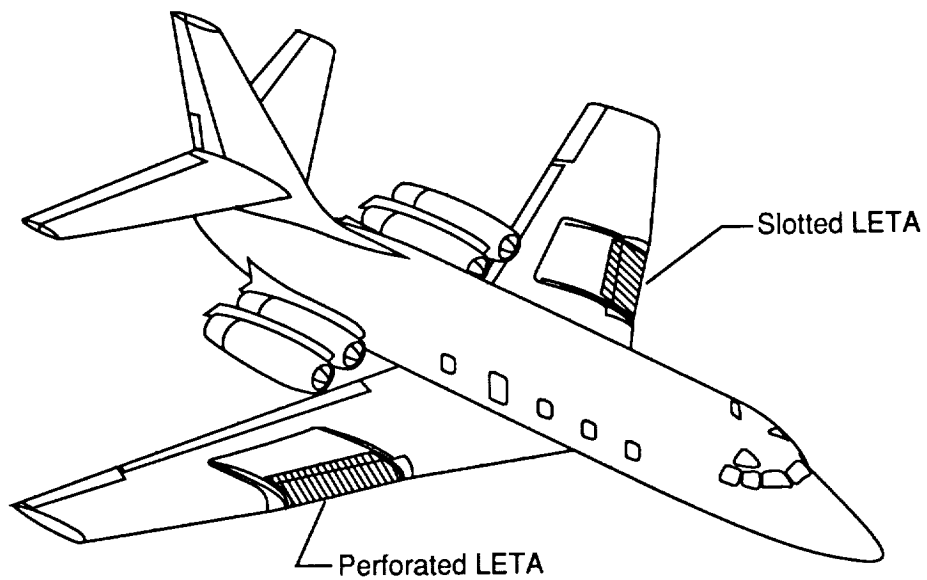
Figure 2. NASA JetStar airplane with leading-edge test articles (LETA's). Dorsal pylon omitted for clarity.
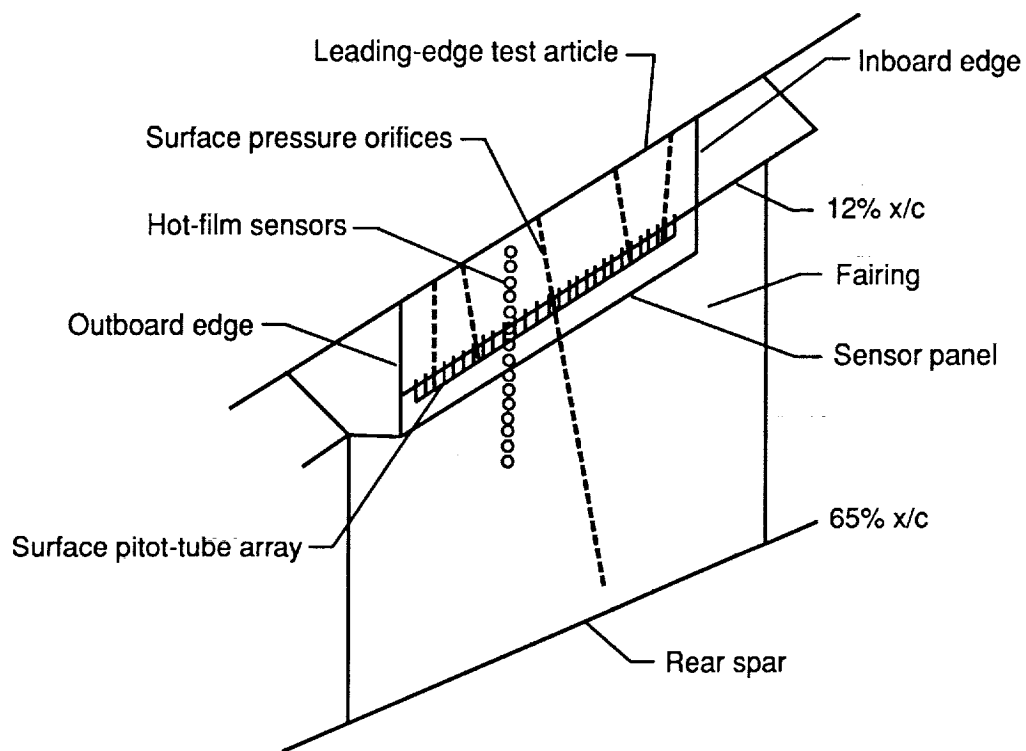
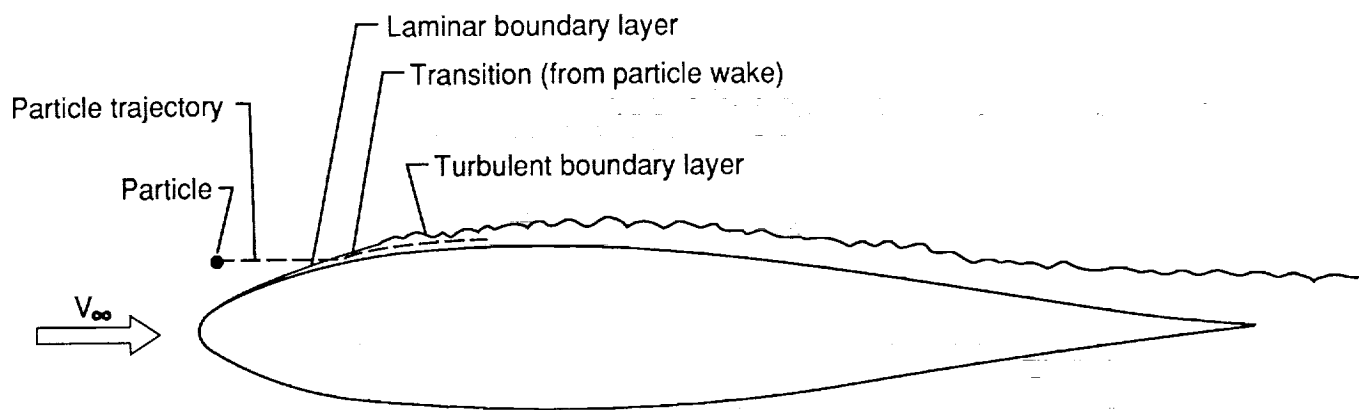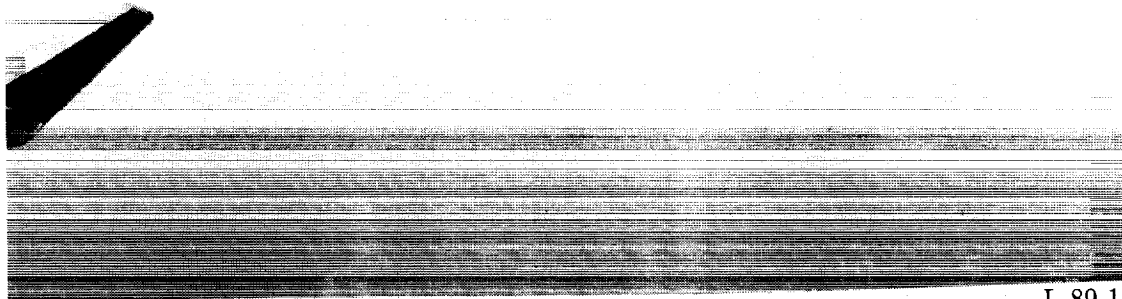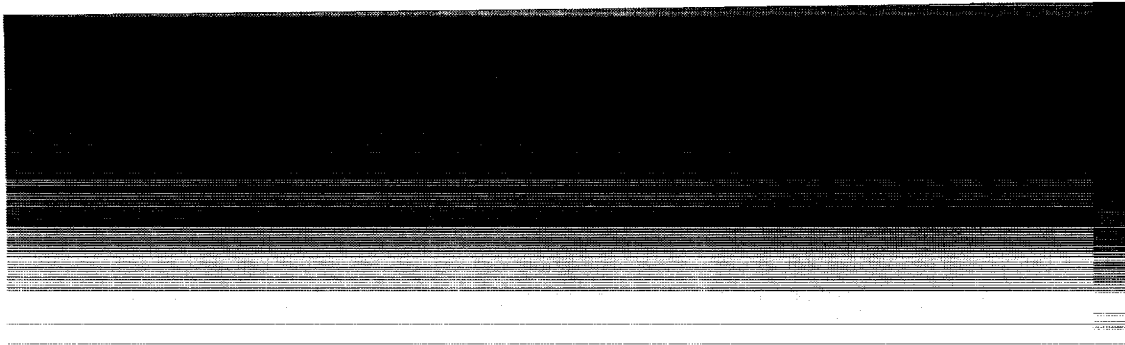Figure 3. Typical arrangement and locations of LFC instrumentation on JetStar glove (left wing shown).

Figure 4. Particle degradation of laminar flow.

L-89-16

(a) 9:24:00 local time, 100% LF.

L-89-17

(b) 9:33:00 local time, 80% LF.

Figure 5. Example of haze conditions affecting laminar flow. Flight 1099.

41

Figure 6. Cloud particle detectors on JetStar pylon.

Knollenberg probe

Charging patch

L-89-18

42
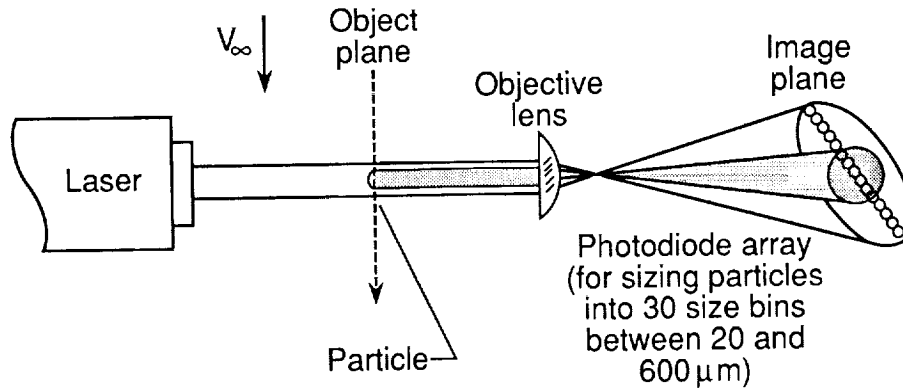
(a) Principle of operation.
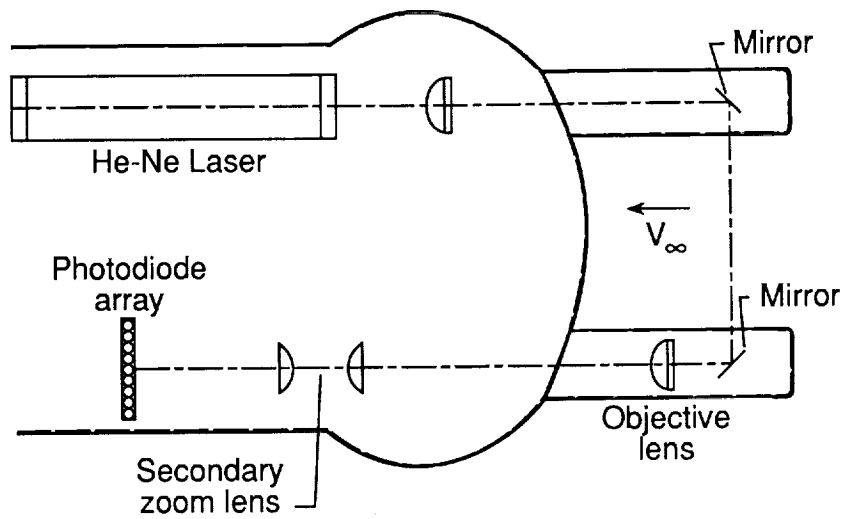
(b) Probe optical system.

L-89-19
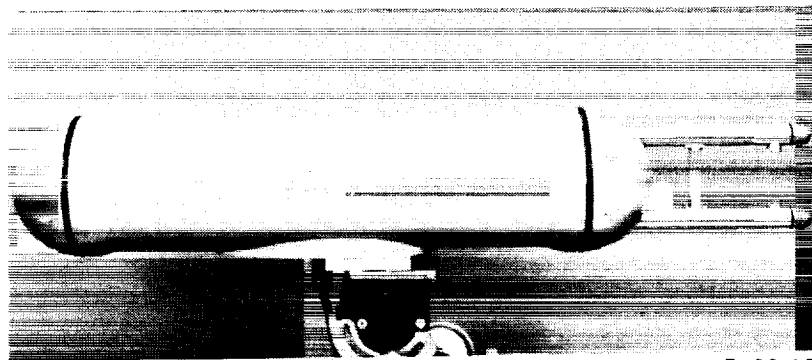
(c) Probe in housing.

Figure 7. Optical array spectrometer (Knollenberg probe).

43
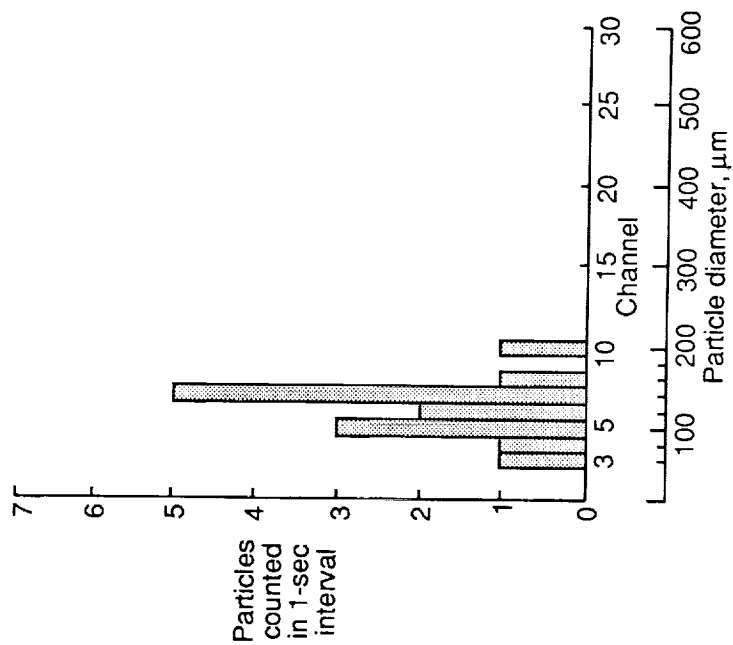
(a) Particle count at 15:54:30.
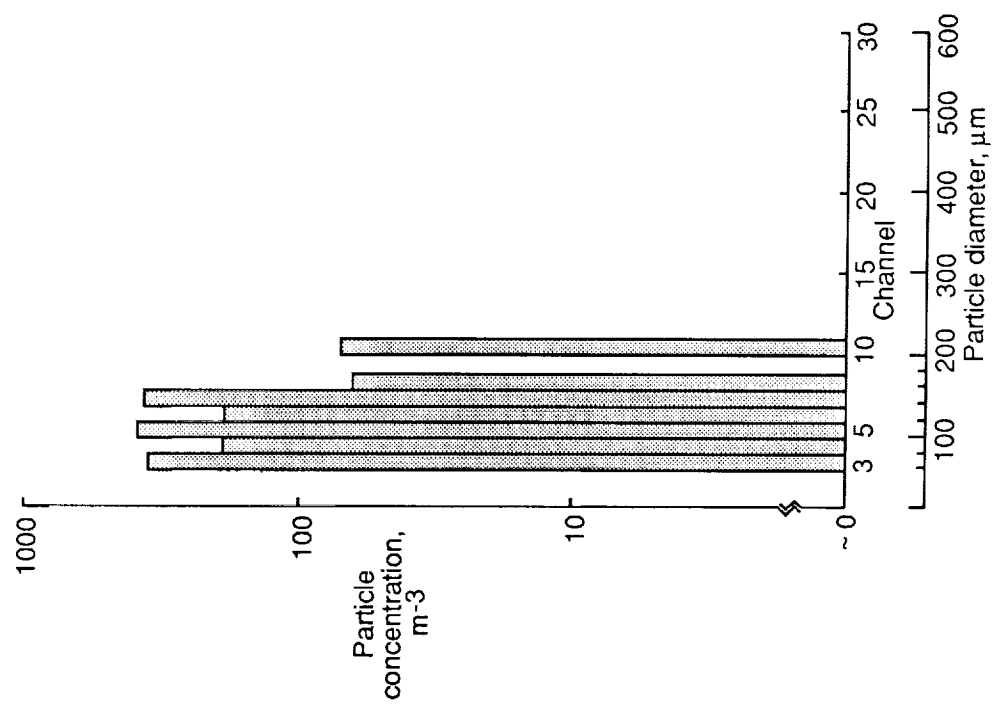
(b) Particle concentration computed from (a).

Figure 8. Example of data obtained with Knollenberg probe on flight 1061.

44
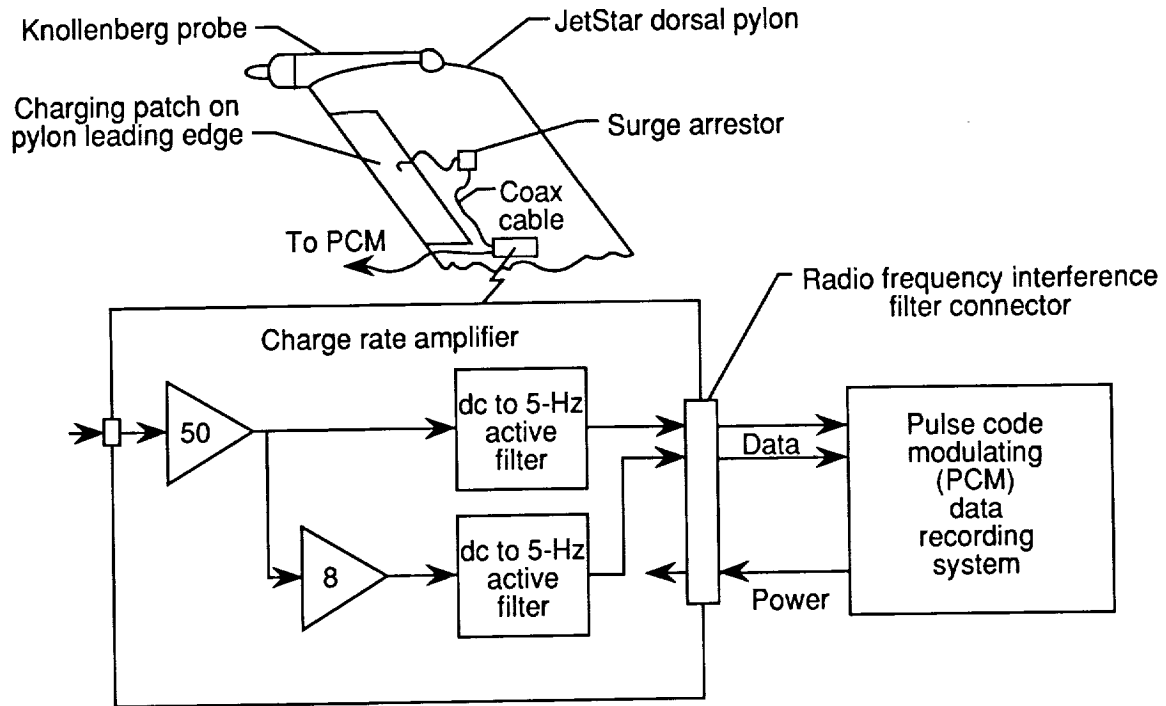
Figure 9. Block diagram of charging-patch cloud particle detector.
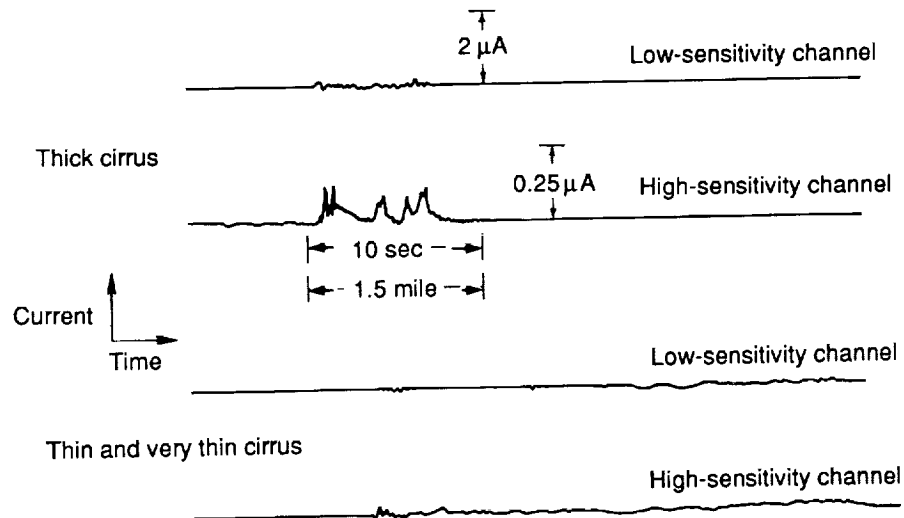
Figure 10. Readings from charging patch in thick and thin cirrus (from prototype instrument aboard F-106B aircraft).
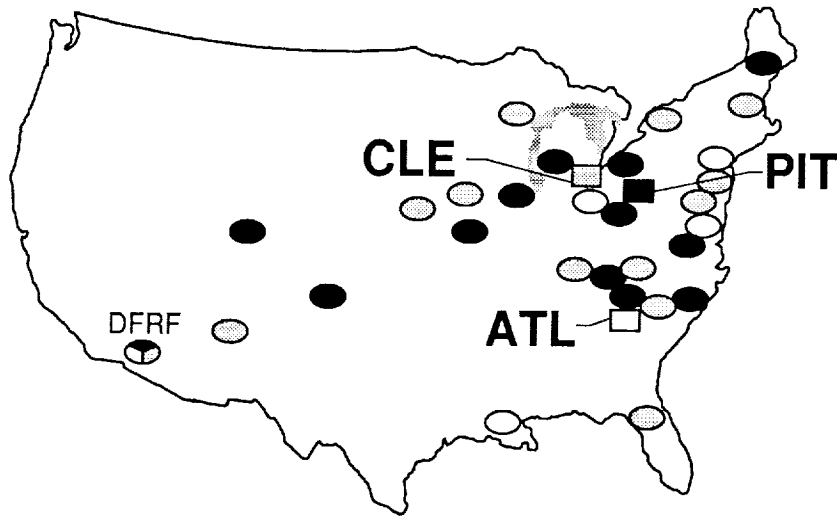
Home base	Date	Number of flights
☐ Atlanta	July 1985	13
■ Pittsburgh	Sept. 1985	26
☐ Cleveland	Feb. 1986	23

Based at 3 major airports; flown in/out of 33 airports; 62 flights total

Figure 11. Airports in Simulated Airline Service Program.

Parent population
all 62 SAS flights
Realism
Availability of data

19 flights chosen for

Aircrew notes on cloud, haze
LF variability on quick-look records
Charge variability on quick-look records

43 flights not analyzed because

39 { Not interesting on quick look
(i.e., LF 100%, constant)
Not interesting on crew
notes
2 Crew notes on LF anomalies
(e.g., icing at probes)
2 Other anomalies

From 19 selected flights: 37008 sec of data (10.28 hr), ≈26% of total cruise time in SAS program

3 ATL out of 13 total ATL
9 PIT out of 26 total PIT
7 CLE out of 23 total CLE
———
19 SAS analyzed out of 62 total

Figure 12. Rationale for selecting data for analysis.
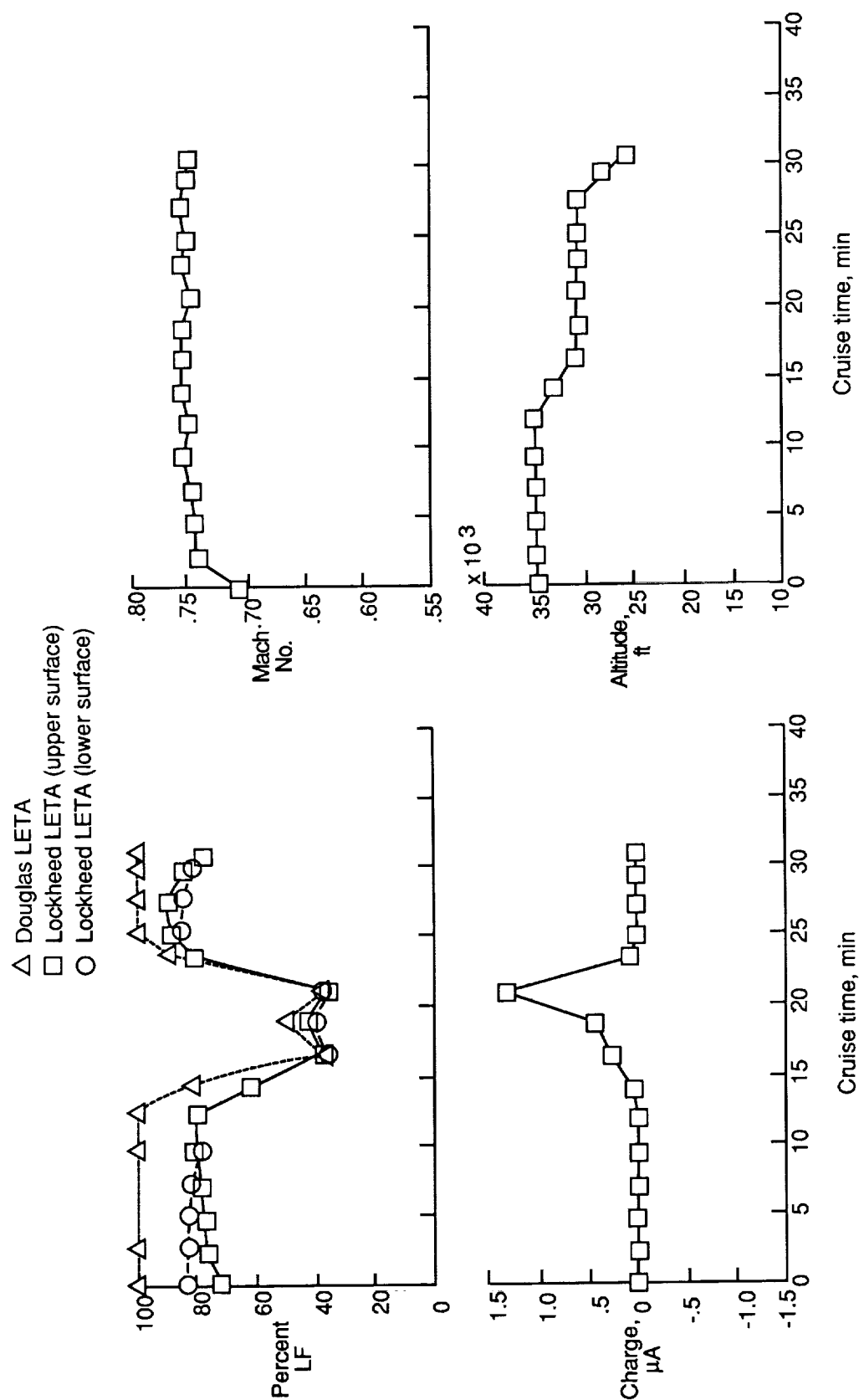
Figure 13. Example of quick-look data.
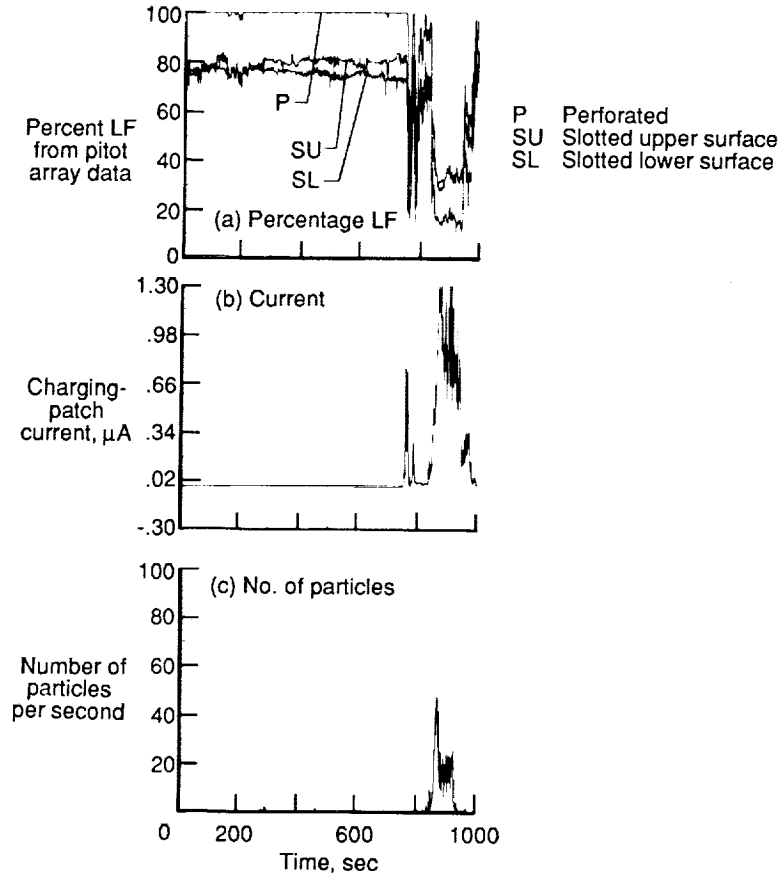
Figure 14. Example of concurrent traces of laminar-flow percentage, charging-patch current, and particle count for flight 1099. $M_\infty = 0.75$; $h_p = 30\,000$ ft.
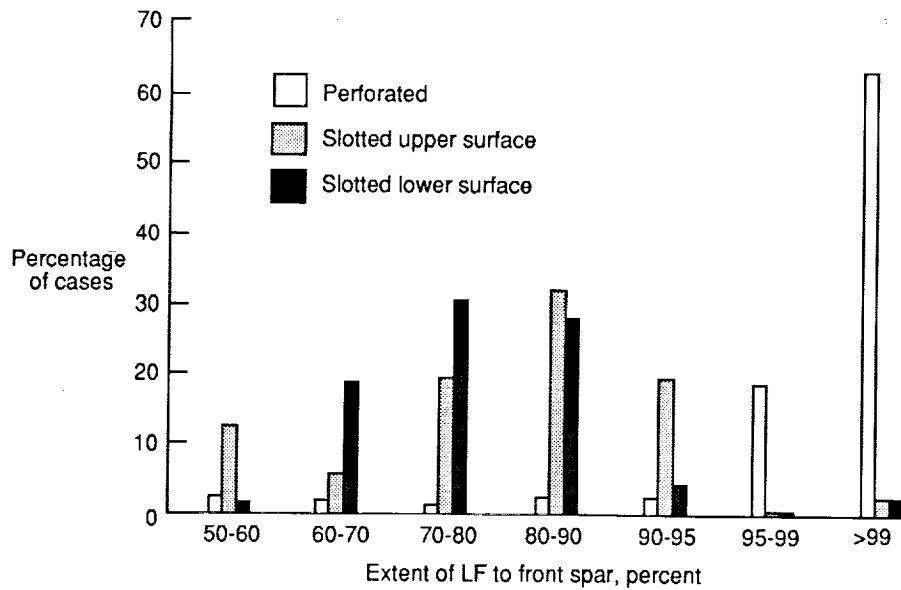

Figure 15. Distribution of laminar-flow values for 11 SAS missions in Atlanta and Pittsburgh deployments (20 258 data points) for both slotted and perforated LETA's.
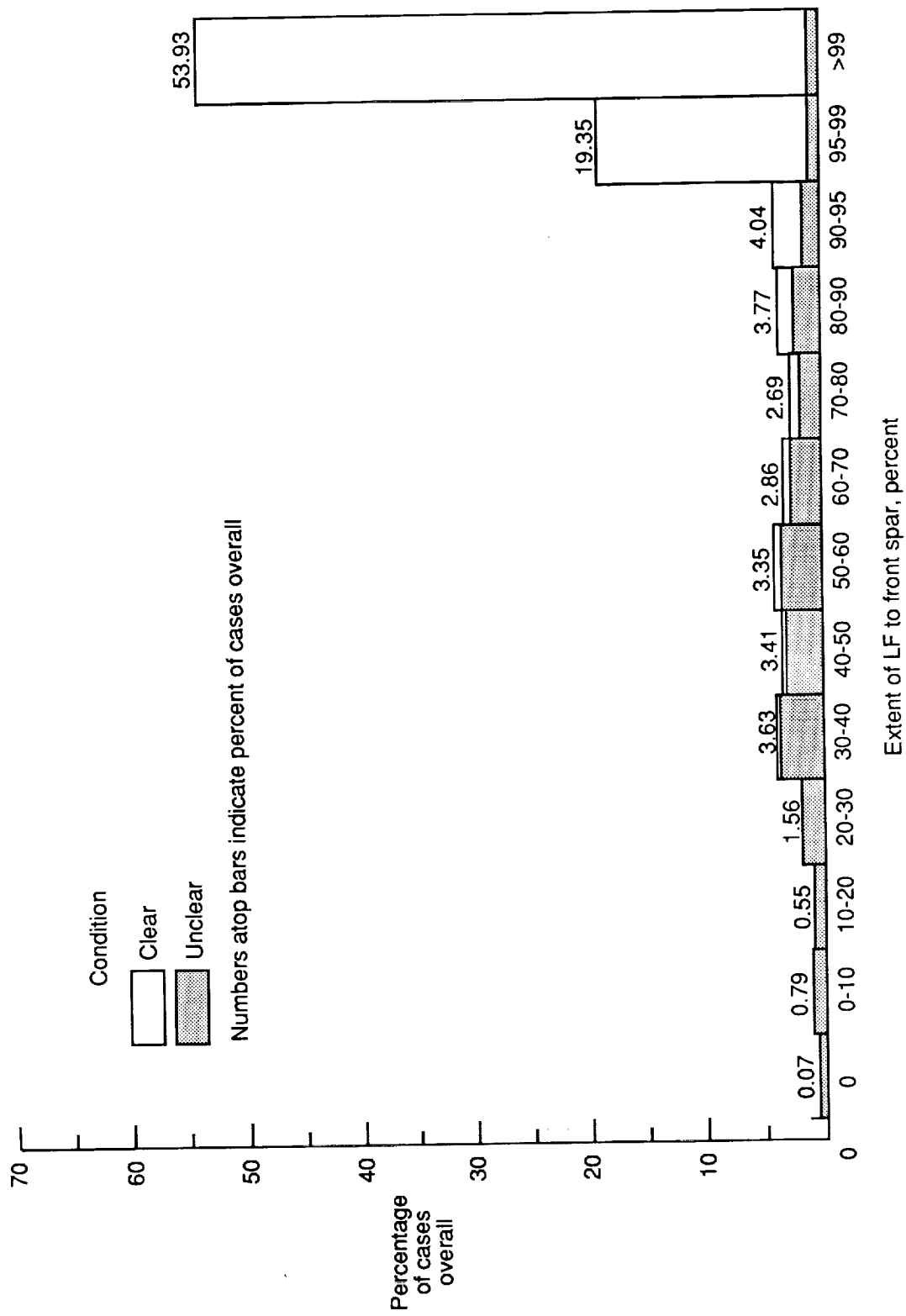
Figure 16. Distribution of laminar-flow values for perforated LETA for entire 19-mission sample (37 008 data points (10.28 hr)) for clear air, unclear air, and overall conditions as determined by charging-patch readings.
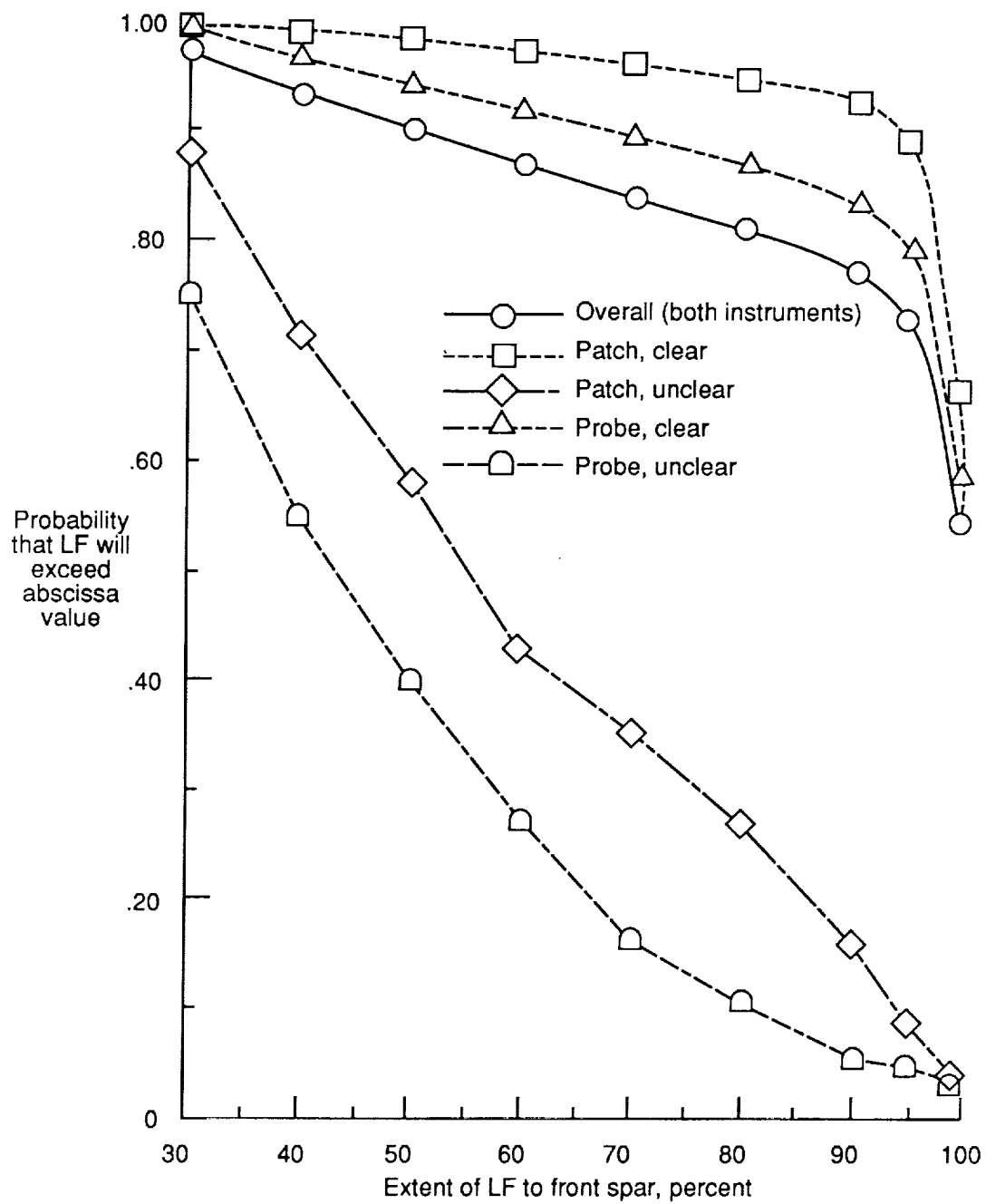
Figure 17. Cumulative frequency distributions of laminar flow in clear air and in unclear air for both Knollenberg probe and charging-patch instruments.
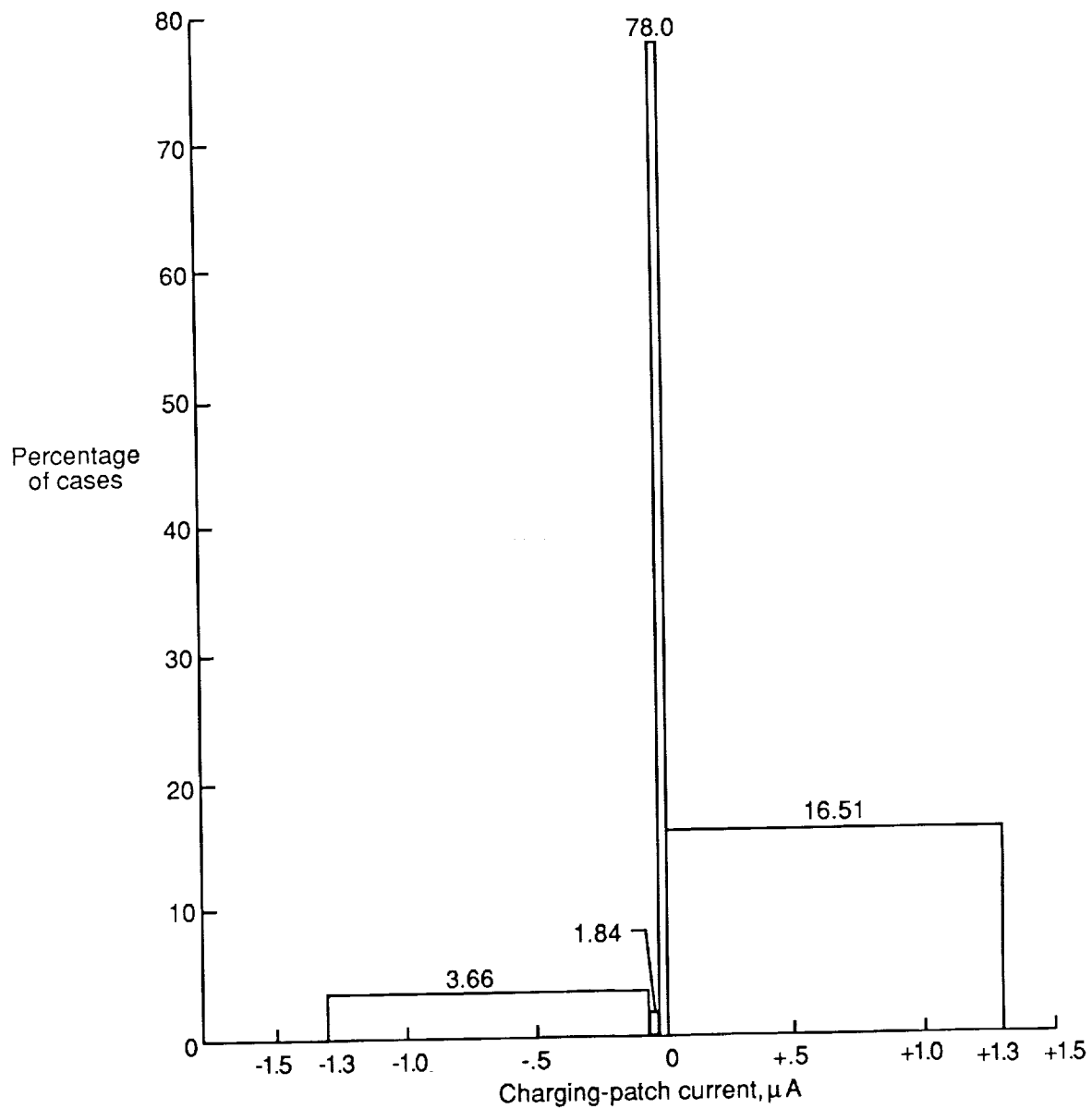
Figure 18. Distribution of charging-patch currents encountered in the 19-mission sample. Numbers atop bars indicate percent of cases overall.
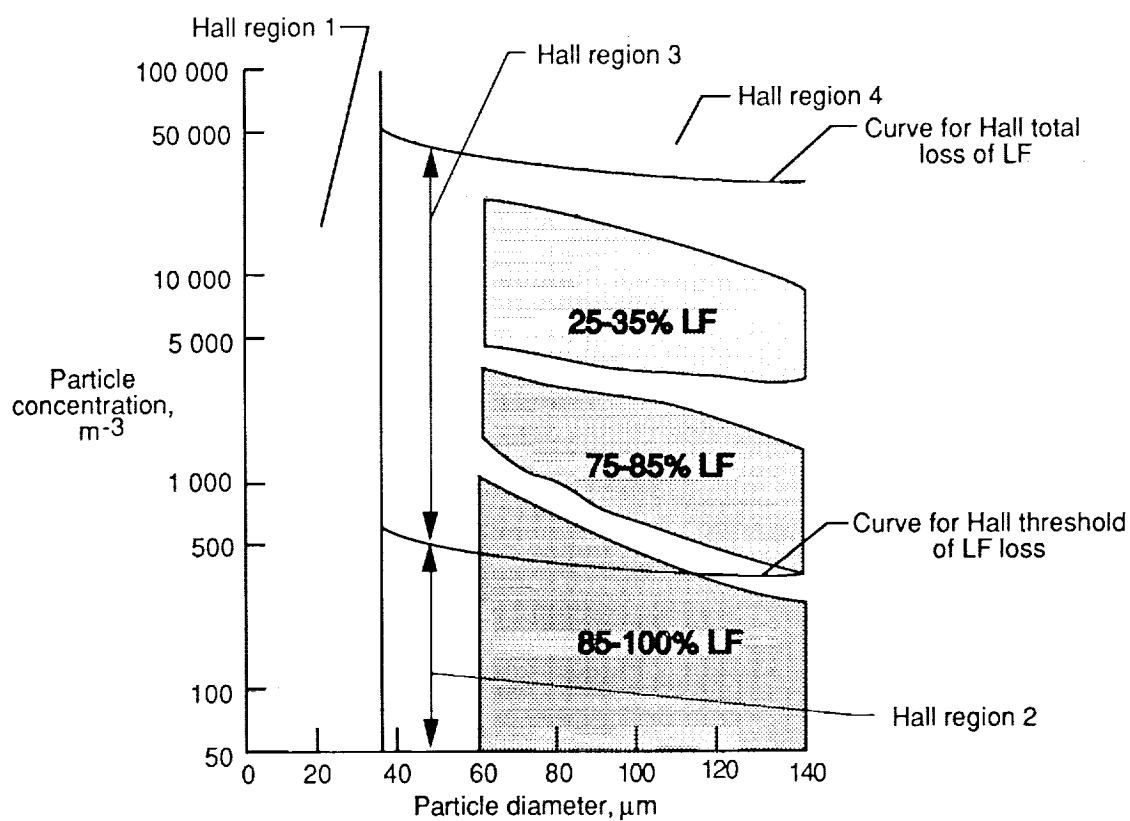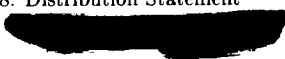
Figure 19. Example of validation of Hall criteria.

1. Report No. NASA TP-2888	2. Government Accession No.	3. Recipient's Catalog No.
4. Title and Subtitle Evaluation of Cloud Detection Instruments and Performance of Laminar-Flow Leading-Edge Test Articles During NASA Leading-Edge Flight-Test Program		5. Report Date April 1989
		6. Performing Organization Code
7. Author(s) Richard E. Davis, Dal V. Maddalon, Richard D. Wagner, David F. Fisher, and Ronald Young		8. Performing Organization Report No. L-16509
9. Performing Organization Name and Address NASA Langley Research Center Hampton, VA 23665-5225		10. Work Unit No. 505-60-31-01
		11. Contract or Grant No.
12. Sponsoring Agency Name and Address National Aeronautics and Space Administration Washington, DC 20546-0001		13. Type of Report and Period Covered Technical Paper
		14. Sponsoring Agency Code

15. Supplementary Notes

Richard E. Davis, Dal V. Maddalon, and Richard D. Wagner: Langley Research Center, Hampton, Virginia.
David F. Fisher and Ronald Young: Ames Research Center, Dryden Flight Research Facility, Edwards, California.

16. Abstract

Summary evaluations of the performance of laminar-flow control (LFC) leading-edge test articles on a NASA JetStar aircraft are presented. Statistics presented for the test articles' performance in haze and cloud situations, as well as in clear air, show a significant effect of cloud particle concentrations on the extent of laminar flow. The cloud particle environment was monitored by two instruments—a cloud particle spectrometer (Knollenberg probe) and a charging patch. Both instruments are evaluated as diagnostic aids for avoiding laminar-flow detrimental particle concentrations in future LFC aircraft operations. The data base covers 19 flights in the simulated airline service phase of the NASA Leading-Edge Flight-Test (LEFT) Program.

17. Key Words (Suggested by Authors(s)) Laminar-flow control Cloud particle instrumentation Environmental effects on aircraft economy Simulated airline service	18. Distribution Statement Subject Category 05
19. Security Classif. (of this report) Unclassified	20. Security Classif. (of this page) Unclassified	21. No. of Pages 57	22. Price